ELSEVIER

Atmospheric Research 62 (2002) 71–109

ATMOSPHERIC RESEARCH

www.elsevier.com/locate/atmos

Investigations on the impact of explicitly predicted snow metamorphism on the microclimate simulated by a meso-β/γ-scale non-hydrostatic model

Kristina Fröhlich [a], Nicole Mölders [b,*]

[a] *Institut für Meteorologie, Universität Leipzig, Stephanstr. 3, 04103 Leipzig, Germany*
[b] *Geophysical Institute, University of Alaska Fairbanks, 903 Koyukuk Drive, P.O. Box 757320, Fairbanks, AK 99775-7320, USA*

Received 21 June 2001; accepted 29 December 2001

Abstract

A snow model is developed, coupled to and tested within the framework of the meso-β/γ-scale non-hydrostatic model, Geesthacht's simulation model of the atmosphere (GESIMA). An evaluation of the snow model is conducted both in a stand-alone version and within GESIMA. In the stand-alone mode, it is evaluated at local scales using data routinely observed at Brandis (51.32°N, 12.62°E, 133 m NN, Saxony) between 1993 and 1997. The snow model reproduces reasonably the temporal evolution of the snow depth; however, it slightly underestimates snow depth, on average. In the coupled mode, simulations are performed with and without the snow model for a winter-storm snow event and a melt period in East Germany to examine the influence of explicitly modeled snow metamorphism on the simulated microclimate. The snow model reasonably predicts the effects typically associated with snow cover. Accuracy of predicted snow depth and extension depends on the lateral boundary conditions and snow prediction by the host model. Evaluation of the simulated air temperatures as well as humidity shows that the inclusion of the snow model improves the model performance as compared to the simulations without snow model. The results show that changing only the values of albedo and emissivity to those typical for snow, as often done in meso-β/γ-scale modeling of snow events, can even lead to opposite effects in simulated latent heat fluxes, ground heat fluxes, soil- and near-surface air temperatures than those typically associated with a snow cover. A rigorous evaluation of the snow simulations in coupled meso-β/γ-scale non-hydrostatic models requires datasets of snow properties (e.g., albedo and emissivity, snow cover extent, snow depth, snow water equivalent, snow temperature) in a high quality and resolution for the region under study. The available datasets are not yet ready to fulfil this objective.

Keywords: Snow metamorphism; Microclimate; Meso-β/γ-scale non-hydrostatic model

* Corresponding author. Tel.: +1-907-474-7910; fax: +1-907-474-7290.

0169-8095/02/$ - see front matter
PII: S0169-8095(02)00005-4

1. Introduction

Over the last decade, in numerical modeling, there has been an increasing interest in using land-surface models (LSM) to provide improved representations of time-varying boundary conditions at the land–atmosphere interface. To guarantee a wide range of applicability, such LSMs have to become increasingly complex and realistic in their representations of meteorology and hydrology (e.g., Gao et al., 1996) and they have to include processes that occur only temporally or in some regions. Since large areas of the continents are subject to seasonal or permanent snow cover and because of the various aspects of snow, there were large affords to consider snow cover in general circulation models (GCM; e.g., Dickinson et al., 1993; Loth et al., 1993; Marshall et al., 1994; Lynch-Stieglitz, 1994; Yang et al., 1997; Slater et al., 1998; Essery et al., 1999). Snow cover, namely, affects temperature and moisture in the soil beneath, trace gas, water and energy budgets, and, hence, modifies air and water quality, watershed hydrology, regional and possibly remote climate (e.g., Yeh et al., 1983; Segal et al., 1991; Dingman, 1994; Yang et al., 1997).

Snow results in a more stable stratification of the atmospheric boundary layer (ABL) and a reduced vertical exchange of trace gases. The depth of snow regulates soil freezing (e.g., Flerchinger, 1991) with implications for soil hydraulic properties and over winter survival of some plants (e.g., Kongoli and Bland, 2000). The reduced hydraulic conductivity of frozen soil increases the potential for high snowmelt runoff losses (e.g., Cherkauer and Lettenmaier, 1999).

Albedo dramatically changes when snow falls and rests on the ground, especially, where the underlying ground has albedo below 0.15 when wet (e.g., Oke, 1978; Pielke, 1984). Since the albedo associated with snow cover typically ranges between 0.35 and 0.9 (e.g., Oke, 1978; Pielke, 1984), the coupling between the surface and atmosphere is generally weaker than under snow-free conditions or in summer.

Variations in the timing and duration of the seasonal snow cover have significant influence on macro- and microclimate conditions through the surface energy balance (e.g., Zhang et al., 2001). Disappearance of snow removes a critical constraint on both water-vapor pressure and surface temperature. As long as the snowpack exists, these quantities cannot rise above 610 Pa and 273.15 K. Therefore, the surface–atmosphere coupling should proceed with more vigor after the melting of snow (Baker et al., 1999). Exposed soil surfaces within a partly broken snow coverage lead to substantial sensible heat fluxes, convection and increased vertical mixing in the surface layer. If sufficient moisture is available, clouds may form. The cloud shadows may feed back to a reduced melt process. The strongly spatial contrast in the energy budget of snow-covered and snow-free areas may lead to significant advective flow similar to a sea breeze (Baker et al., 1999). Furthermore, snowmelt releases the trace constituents accumulated in the snowpack over the snow period into the ecosystems within a short time (e.g., Dingman, 1994).

Due to these various aspects of snow, it is of great interest to include snow models also in meso-β/γ-scale non-hydrostatic models for air pollution or hydrometeorological studies on the local scales. While in hydrological and glaciological applications, the aspects of forecasting the water-cycle-related quantities (e.g., flood warning, reservoir management, the coordination of power distribution, water quality, etc.) or processes within the snowpack (snow metamorphism) are in the center of interest (e.g., Blöschl and Kirnbauer,

1991) additional aspects have to be considered in snow models for atmospheric models. In GCMs or meso-β/γ-scale non-hydrostatic models, the computational limitations do not allow to treat the internal snow processes in every detail like in the essentially complete physically based snow model of Anderson (1976), for instance. This research snow model included, among other things, snowpack accumulation, change of albedo, settling and compaction, snowmelt, meltwater retention and percolation as well as the snowpack energy balance. Furthermore, the time steps typical for GCMs or meso-β/γ-scale non-hydrostatic models do not allow coarse approaches like the day–degree method wherein snowmelt depends on daily mean temperature.

Therefore, depending on the intended application one (e.g., Verseghy, 1991; Dickinson et al., 1993; Douville et al., 1995), two (e.g., Rodriguez, 1999) or multiple layer snow models (e.g., Loth et al., 1993; Lynch-Stieglitz, 1994) of different degrees of complexity were developed especially for the purposes required by GCMs. Simple one-layer snow models assume a homogenous snowpack and work with the energy budget. Some of them allow that the snowpack covers only a fraction of the grid cell. Thermal conductivity and volumetric specific heat of snow and the composite soil snow layer often depend on the snow age and fraction of the grid cell covered by snow (e.g., Dickinson et al., 1993). If snow temperature achieves the freezing point, further energy input will lead to snowmelt. Outflow sets on after the retention capacity is exceeded. Obviously, these simplifications will lead to unrealistic results for thick snowpacks and if thaw–freezing cycles occur frequently because, in these cases, the snowpack is far beyond being homogeneous (e.g., Loth, 1995). This shortcoming is overcome by two-layer snow models. The snowpack is divided into a dry upper and a wet lower layer during melt episodes where the frost depth determines the boundary between the two layers. The lower layer is assumed to be isotherm at 273.16 K. Meltwater outflow is retarded by the water-holding capacity of the lower snow layer. Loth et al. (1993) and Lynch-Stieglitz (1994) developed independently from each other multiple-layer snow models for use in GCMs taking into account the snow density, snow temperature and snow water equivalent. Usually, no link to the vegetation soil system is considered. Such a link, however, exists in the one-layer snow model of Biosphere–Atmosphere Transfer Scheme (BATS), e.g., where 15 vegetation types are taken into account and a common temperature of soil and snow is determined (e.g., Dickinson et al., 1993). In meso-β/γ-scale non-hydrostatic models, snow processes are usually ignored and snow is only represented by a change in albedo and emissivity (e.g., Eppel et al., 1995) if at all.

Up to now, it is unknown how detailed the physical processes within a snowpack can be determined and which degree of complexity is required in snow models for use in atmospheric models (e.g., Yang et al., 1997; Slater et al., 2000). Comparison of the climatic response to snow in 17 different GCMs showed both strong alterations to changes in snow regime as well as limited climatic response due to negative feedbacks (Cess et al., 1991). Foster et al. (1996) undertook a comparison of the snow water equivalent produced by seven GCMs and found consistency between them, but a wide variety in the magnitude and temporal distribution within the transitional seasons. These differences were mostly attributed to mispredictions in precipitation and temperature fields. A comparative study of (1) a snow model which uses a mixture theory to simulate multiphase water and energy transfer processes in the snow layers, (2) a simplified three-layer snow model, and (3) a snow model which calculates snowmelt from the energy budget and snow temperature by

the force–restore method showed that all these models simulated times series of snow water equivalent, surface temperature and fluxes very well, with the first-mentioned giving the best match, but needing the highest computational efforts. The second one approximately performs like the first one; however, it has computational requirements comparable to the third-mentioned snow model (Jin et al., 1999). The comparisons of various stand-alone versions of snow models carried out within the framework of the Project for Intercomparison of Land Parameterization Schemes (PILPS) demonstrated that the LSMs applied and other parameters (e.g., albedo, heterogeneity, etc.) than the number of snow layers also influence the results of the snow models (Slater et al., 2000). In the framework of PILPS, a greater sensitivity of ablation of the winter snowpack to the choice of snow parameterization was found as compared to the accumulation (Schlosser et al., 2000). A detailed review on snowmelt modeling for a variety of climatic conditions can be found in Leavesley (1989).

Our paper presents a semicomplex physically based multiple-layer snow model to describe snow metamorphism in the meso-β/γ-scale meteorological model, Geesthacht's simulation model of the atmosphere (GESIMA); Kapitza and Eppel, 1992; Eppel et al., 1995). In GESIMA, the snow model is coupled to the LSM developed by Claussen (1988) and modified by Mölders (1998). Simulations are exemplary performed with and without the snow model for a snow accumulation and a melt period in East Germany (Fig. 1) to investigate the impact of explicitly simulated snow physical processes on the local microclimate. Special focus is on the effects caused by the simplification of just changing albedo and emissivity, which is commonly applied to represent snow in meso-β/γ-scale non-hydrostatic models. The simulation results are evaluated by means of observations where available. The general performance of the snow model is also demonstrated by means of analytical solutions as well as snow depth data that were routinely observed at Brandis (southeast of Leipzig, 51.32°N, 12.62°E, 133 m NN, Saxony) between 1993 and 1997.

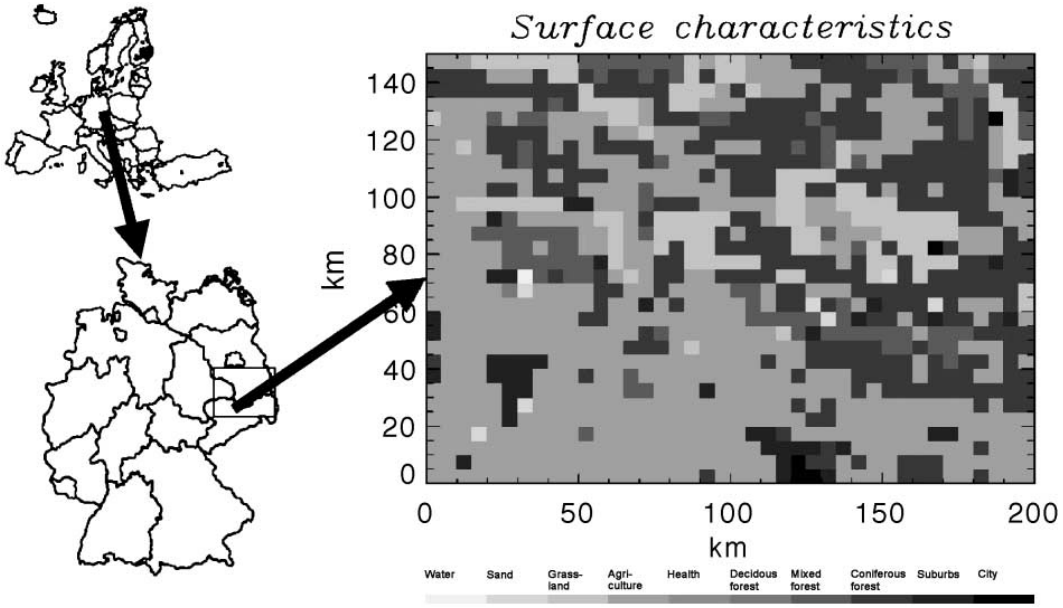

Fig. 1. Location of the model domain in Europe and Germany as well as distribution of land-use types.

2. Brief description of the meso-β/γ-scale non-hydrostatic model GESIMA

The main dynamical, numerical and physical features of GESIMA are given in Kapitza and Eppel (1992) and Eppel et al. (1995). However, the model physics used in our study differs from that described by these authors by (1) the determination of the surface stress and near-surface fluxes of heat and water vapor by use of Kramm et al.'s (1995) parametric model wherein these fluxes are expressed in terms of dimensionless drag coefficients and transfer coefficients of heat and moisture; (2) the modifications of GESIMA's LSM (see Mölders, 1998); (3) the inclusion of the newly developed snow model described in Section 3; and (4) the treatment of cloud microphysics by a modified version of the five water-class bulk parameterization scheme, which includes water vapor, cloud water, rainwater, ice and graupel (e.g., Mölders et al., 1997). This parameterization was adapted for application in winter conditions. Herein, the settling of ice crystals starts after the ice

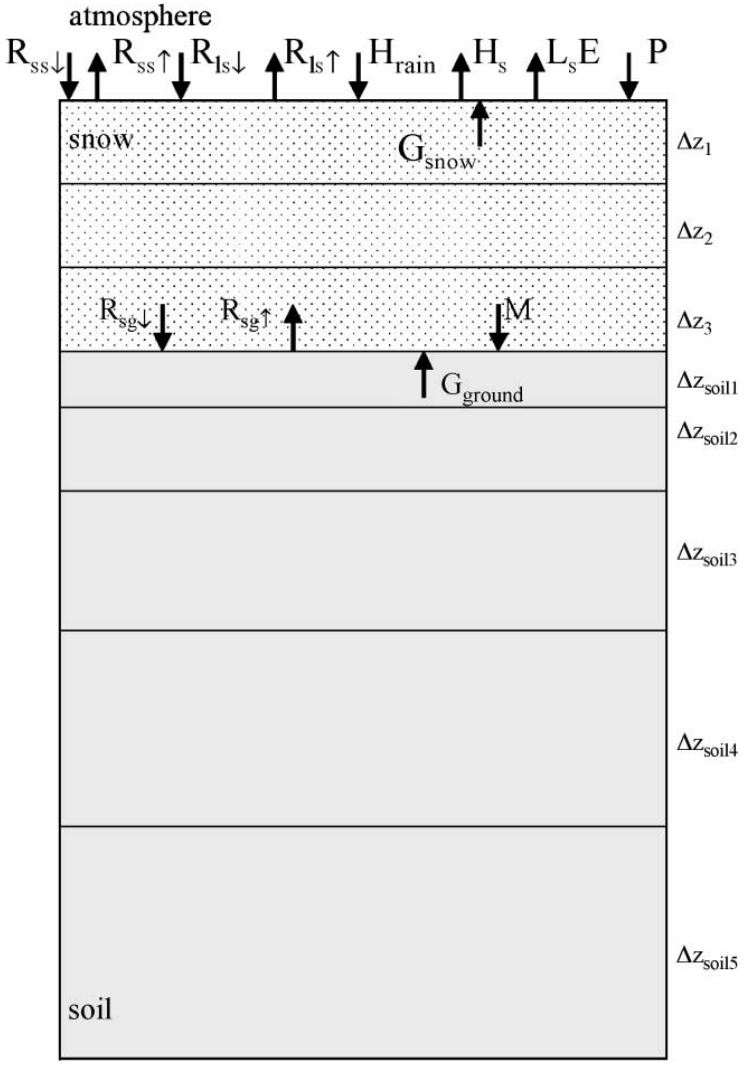

Fig. 2. Schematic view of snow model coupled to the LSM and GESIMA. See text for explanation of symbols.

mass exceeds a critical value of 10^{-9} kg per unit volume, i.e., below this value ice is considered as cloud ice. Moreover, the graupel-like snow of hexagonal type, which occurs more frequently under convective conditions in summer, was substituted by dendrites, which are more common in winter. Note that graupel-like snow of hexagonal type is formed in updrafts by riming of ice particles by cloud droplets, while dendrites are built by water-vapor diffusion onto ice nuclei. From the dynamical and thermodynamical points of view, these modifications mean that the onset of precipitation at the ground is retarded and the atmosphere keeps wetter than in the original version. A graupel-like snow particle of hexagonal type with 0.002 m in diameter, for instance, settles with a terminal velocity of 1.63 m/s, while a dendrite of same size falls at 0.95 m/s. For a detailed discussion of the impact of cloud ice, see Mölders et al. (1995).

At the lateral boundaries, the Orlanski (1976) radiation-boundary condition is applied for the normal component of momentum, and a zero-gradient method is used for all other variables except for cloud and precipitating particles that are assumed to be zero, i.e., no advection of clouds and precipitation into the model domain occurs. At the top of the model, a rigid lid, together with a sponge layer to absorb vertically propagating gravity waves, are applied. More details of the model configuration can be found in Mölders (1998, 1999a,b, 2000).

GESIMA and its modules have been evaluated for a wide range of applications (e.g., Claussen, 1988; Kapitza and Eppel, 1992; Levkov et al., 1992; Eppel et al., 1995; Devantier and Raabe, 1996; Hinneburg and Tetzlaff, 1996; Mölders, 1998; 1999a; Raabe and Mölders, 1999). Moreover, GESIMA has shown itself able to model atmospheric responses to surface characteristics usually observed (e.g., Eppel et al., 1995; Mölders, 1998).

3. Description of the snow metamorphism model

Fig. 2 shows a schematic view of the multiple-layer snow model developed for our study. It considers snow layers of time varying depth. The thickness, Δz, of these layers is related to the total snow depth, h_s, by (Fröhlich, 2001):

$$h_s = \sum_{j=1}^{n} \Delta z_j, \tag{1}$$

where n is the amount of snow layers ($=3$ in our study). Snow depth increases by snowfall and decreases by snow metamorphism processes, namely, (1) breaking of snow crystals by wind blow, increase of snow density by (2) compaction, (3) settling, and (4) percolation as well as (5) freezing of meltwater.

3.1. Wind break

At $t=0$, according to the cloud module (Mölders et al., 1997), initial density of snow, $\rho_{s,\mathrm{input}}^{t=0}$, amounts to 84 kg/m^3. Wind blow breaks down the snow crystals for which the

density increases at the snow surface (see Table 1). At time t, the density of the uppermost snow layer is determined by (Fröhlich, 2001):

$$\rho_{s,1}^{t} = \frac{\rho_{s,\mathrm{input}}^{t}\Delta h + \rho_{s,1}^{t-1}(\Delta z_1 - \Delta h)}{\Delta h + \Delta z_1}, \tag{2}$$

where $\rho_{s,\mathrm{input}}^{t}$ depends on wind speed (see Table 1). Furthermore, $\rho_{s,1}^{t-1}$, Δh, and Δz_1 are the density of the uppermost snow layer in the time step before, the height of snow fallen since the last time step, and the thickness of the uppermost snow layer. In the following, the indices for time and snow layers are dropped for simplicity.

3.2. Compaction

The compaction of snow depends on the overlying snow mass and is given for each layer by (e.g., Mellor, 1964; Anderson, 1976):

$$\frac{1}{\rho_s}\frac{\partial \rho_s}{\partial t} = \frac{g}{v_c}\int_{h_s}^{z} \rho_s \mathrm{d}z, \tag{3}$$

where g is the acceleration of gravity. The viscosity coefficient, v_c, depends on the density and temperature of snow, T (e.g., Anderson, 1976):

$$v_c = v_0 \exp(C_1(T_0 - T))\exp(C_2\rho_s)), \tag{4}$$

with the compaction parameter $C_2 = 2.1\cdot 10^{-2}$ m^3/kg. Furthermore, $C_1 = 0.08$ K^{-1}, $T_0 = 273.15$ K, and $v_0 = 3.7 \times 10^7$ Pa s.

3.3. Settling

In each layer, destructive metamorphism by settling is calculated by (Anderson, 1976):

$$\frac{1}{\rho_s}\frac{\partial \rho_s}{\partial t} = \begin{cases} C_3 \exp(-C_4(T_0 - T))\exp(-46\cdot 10^4(\rho_s - pt\rho_c)) & \rho_s \geq \rho_c \\ C_3 \exp(-C_4(T_0 - T)) & \rho_s < \rho_c \end{cases} \tag{5}$$

with the empirical parameters $C_3 = 2.8\cdot 10^{-7}$ s^{-1}, $C_4 = 0.04$ K^{-1} and the critical snow density value, ρ_c ($= 150$ kg/m^3).

3.4. Snow temperature, snowmelt and refreezing

Snow flakes falling onto the snowpack are assumed to have the same temperature as the surrounding air (Fröhlich, 2001). Assuming that the Dufor effect (i.e., a moisture gradient may alter snow temperature) and Ludwig–Soret effect (i.e., a temperature gradient is able

Table 1
Dependence of change in snow density, $\rho_{s,\mathrm{input}}^{t}$, on wind speed, v, for the uppermost snow layer

v (m/s)	<0.24	0.24–0.40	0.40–0.50	0.50–0.60	>0.60
$\rho_{s,\mathrm{input}}^{t}$ (kg/m^3)	84	160	270	330	440

to generate a change of the volumetric liquid water content of the snowpack) are negligible for the typical duration of snowpacks in mid-latitudes, the equations for the transport of heat and water within the snowpack can be decoupled. The heat transport within the snowpack is calculated for each model layer by the heat diffusion equation (e.g., Anderson, 1976):

$$C_s \frac{\partial T}{\partial t} = \lambda_s \frac{\partial^2 T}{\partial z^2}, \tag{6}$$

where C_s and λ_s are the volumetric heat capacity and the thermal conductivity of snow. These thermal properties depend on snow density (e.g., Anderson, 1976):

$$C_s = c_i \rho_s, \tag{7}$$

$$\lambda_s = 0.02 + 2.5 \cdot 10^{-7} \rho_s^2. \tag{8}$$

Here c_i ($=2105$ J kg^{-1} K^{-1}) is the specific heat capacity of ice. Eq. (6) is solved by using the Crank–Nicholson method (Fröhlich, 2001).

In a model layer, snowmelt occurs when its snow temperature exceeds the freezing point, T_0. Further energy supply produces meltwater (see, e.g., Dingman, 1994)

$$w = c_i \rho_s \Delta z \frac{T - T_0}{L_f \rho_w}, \tag{9}$$

where ρ_w ($=1000$ kg/m^3) and L_f are the density of water and the latent heat of fusion, respectively. The maximum value of liquid water, $w_{ret,max}$, that can be held in the snow layer against gravity is determined by (e.g., Dingman, 1994):

$$w_{ret,max} = \left(-0.0735 \frac{\rho_s}{\rho_w} + 0.267 \cdot 10^{-4} \frac{\rho_s^2}{\rho_w} \right) \Delta z. \tag{10}$$

If the snow temperature falls below the freezing point, meltwater will refreeze until either all liquid water is frozen or the freezing point is reached again by the release of heat.

3.5. Percolation

Since wet snow mainly consists of rounded grains of hygroscopic material, the water flow through a homogeneous snow layer can be regarded as a flow through porous media. If liquid water is present, small ice grains will be eliminated quickly by metamorphism until diameters of 10^{-3} to 2×10^{-3} m are achieved. These grains provide a high porosity and reduced capillary potential as compared to small ice grains or most soils. The decrease in capillary attraction with increase of grain size leads to the phenomenon that snow can retain liquid water and then release it suddenly (e.g., Colbeck, 1978). Thus, gravity forces

dominate the water flow through a mature snowpack. Applying Darcy's law leads to the water flux (volume of water per unit area per unit time; Colbeck, 1978):

$$u = \frac{K_w}{\nu_w}\left(\frac{\partial \Psi}{\partial z} + \rho_w g\right). \tag{11}$$

Here, K_w, ν_w ($=1.792 \times 10^{-3}$ kg/(ms)) and Ψ are the permeability, the viscosity of water and the capillary pressure, also often denoted as liquid tension, which is approximately equal to the negative pressure in the water because air pressure is close to atmospheric. The intrinsic permeability of the snowpack is related to that at saturation, K_{ws}, by (Colbeck, 1978):

$$K_w = K_{ws} S_{eff}^{*3} \tag{12}$$

with the effective saturation, S_{eff}^{*}, i.e., the percentage of pore volume occupied by the mobile liquid. In a snow layer, the permeability depends on grain diameter, d, and the snow density of the respective layer (e.g., Siemer, 1988):

$$K_{ws} = 0.077 d^2 \exp\left(-7.8\frac{\rho_s}{\rho_w}\right) \tag{13}$$

with (Wanciewicz, 1978):

$$d = 2 \times 10^{-4} \exp(5 \times 10^{-3} \rho_s). \tag{14}$$

Combining Eqs. (11) and (12) and neglecting the gradient of the hydraulic conductivity provides the flux of water through the unsaturated snow (e.g., Colbeck, 1978):

$$u = \frac{\rho_w g}{\nu_w} K_{ws} S_{eff}^{*3} = \alpha K_{ws} S_{eff}^{*3}, \tag{15}$$

with $\alpha = \rho_w g/\nu_w$. Combing this equation with that of the continuity of water in the snowpack (see Colbeck, 1978):

$$\frac{\partial u}{\partial z} + \Pi_{eff}\frac{\partial S_{eff}^{*}}{\partial t} = 0, \tag{16}$$

and converting it into the flux form yields to (Colbeck, 1978):

$$\frac{\partial u}{\partial z} + \frac{\Pi_{eff}}{3\alpha^{1/3} K_{ws}^{1/3} u^{2/3}}\frac{\partial u}{\partial t} = 0, \tag{17}$$

where the effective porosity of the snow, $\Pi_{eff} = \Pi(1 - S_i)$, is the porosity of snow minus the pore volume filled by retained water. The porosity of snow can be expressed by (Dunne et al., 1976):

$$\Pi = \frac{\rho_s - \rho_i}{S_i \rho_w - \rho_i}. \tag{18}$$

Here, S_i (≈ 0.07 m^3/m^3) is the maximal water saturation of the snowpack and ρ_i ($=916$

kg/m^3) denotes to the density of solid ice. The relationship between the flux of water, u, and the rate of vertical descent of that flux can be determined by (Colbeck, 1978):

$$\left.\frac{\mathrm{d}z}{\mathrm{d}t}\right|_u = \frac{3\alpha^{1/3}K_{\mathrm{ws}}^{1/3}u^{2/3}}{\Pi_{\mathrm{eff}}}. \tag{19}$$

3.6. Energy budgets

The energy budget equation of the snow surface reads

$$R_{\mathrm{ss}\downarrow} - R_{\mathrm{ss}\uparrow} + R_{\mathrm{ls}\downarrow} - R_{\mathrm{ls}\uparrow} - H_{\mathrm{s}} - L_{\mathrm{s}}E + G_{\mathrm{snow}} + H_{\mathrm{rain}} = 0, \tag{20}$$

where $R_{\mathrm{ss}\downarrow}$, $R_{\mathrm{ss}\uparrow}$ ($=\alpha_{\mathrm{s}}R_{\mathrm{ss}\downarrow}$), $R_{\mathrm{ls}\downarrow}$ and $R_{\mathrm{ls}\uparrow}$ ($=\varepsilon_{\mathrm{s}}\sigma T_{\mathrm{s,surf}}{}^4+(1-\varepsilon_{\mathrm{s}})R_{\mathrm{ls}\uparrow}$) are the downward ($\downarrow$) and upward ($\uparrow$) directed fluxes of short-wave and long-wave radiation at the snow surface (Fig. 2). The global radiation, $R_{\mathrm{ss}\downarrow}$, and the long-wave radiation of the atmosphere, $R_{\mathrm{ls}\downarrow}$, are delivered by the radiative transfer model, which uses a two stream method (see Eppel et al., 1995). Furthermore, G_{snow} and H_{rain} represent the snow heat flux and the input of heat by precipitation. The turbulent fluxes of latent, $L_{\mathrm{s}}E$, and sensible heat, H_{s}, are determined in accord with Mölders (1998) under the assumption that the specific humidity at the snow surface is equal to the specific humidity at saturation above ice. The surface temperature of the snowpack is denoted as $T_{\mathrm{s,surf}}$. The albedo, α_{s}, and emissivity, ε_{s}, of snow depend on snow age, t_{snow} (in s), after the last snowfall according to (Mölders et al., 2001):

$$\alpha_{\mathrm{s}} = \begin{cases} 0.35 + 0.18\exp\left(\frac{-t_{\mathrm{snow}}}{114{,}048}\right) + 0.31\exp\left(\frac{-t_{\mathrm{snow}}}{954{,}720}\right) & T_{\mathrm{R}} > 273.15\ \mathrm{K} \\ 0.61 + 0.23\exp\left(\frac{-t_{\mathrm{snow}}}{469{,}411.2}\right) & T_{\mathrm{R}} \leq 273.15\ \mathrm{K} \end{cases}, \tag{21}$$

$$\varepsilon = \max(0.82, 0.99 - 9.8\times 10^{-7}t_{\mathrm{snow}}). \tag{22}$$

Here, T_{R} is the air temperature at reference height (i.e., at the first half level above ground, which is located at a height of 10 m). Mölders et al. (2001) derived Eqs. (21) and (22) from data given by U.S. Army Corps of Engineers (1956; cited in Dingman, 1994).

If snow exists, some radiation will be absorbed by the snowpack. The turbulent fluxes of sensible and latent heat are assumed to be zero at the soil–snow interface. Thus, the energy budget for the ground reads:

$$R_{\mathrm{sg}\downarrow} - R_{\mathrm{sg}\uparrow} + G_{\mathrm{ground}} = 0 \tag{23}$$

with:

$$R_{\mathrm{sg}\downarrow} = R_{\mathrm{ss}\downarrow}\exp(-k_{\mathrm{ext}}h_{\mathrm{s}}), \tag{24}$$

and $R_{\mathrm{sg}\uparrow}$ ($=\alpha_{\mathrm{g}}R_{\mathrm{sg}\downarrow}$). Here, the index g stands for the ground and G_{ground} denotes to the ground heat flux. The albedo of the soil, α_{g}, is taken from Table 2. The extinction coefficient, $k_{\mathrm{ext}} = 7\ \mathrm{m}^{-1}$ in accord with Hermann and Kuhn (1990). This value means that, in the case of a 0.1-m-deep snowpack, for example, only 50% of the downward short-wave radiation flux density reach the ground surface.

Table 2
Thermal diffusivity, k_{soil}, and heat capacity of the soil, $\rho_{soil}c_{soil}$, emissivity, ε_g, and albedo, α_g, of the surface, roughness length, z_0, as used in the model

Land-use type	k_{soil} (10^{-6} m^2/s)	$\rho_{soil}c_{soil}10^6$ (J/m^{3}K)	ε_g	α_g	z_0 (m)
Water	0.15	4.2	0.94	*	*
Sand	0.84	2.1	0.99 (0.99)	0.35 (0.80)	0.0001
Grassland	0.56	2.1	0.99 (0.99)	0.15 (0.35)	0.001
Agriculture	0.74	2.9	0.99 (0.99)	0.15 (0.70)	0.01
Heath	0.70	2.5	0.99 (0.99)	0.25 (0.60)	0.01
Deciduous forest	0.70	2.5	0.95 (0.98)	0.15 (0.60)	0.5
Mixed forest	0.70	2.5	0.95 (0.98)	0.15 (0.60)	0.5
Coniferous forest	0.70	2.5	0.95 (0.98)	0.15 (0.60)	0.5
Village	1.0	2.0	0.95 (0.95)	0.15 (0.40)	0.8
City	1.0	2.0	0.95 (0.95)	0.15 (0.40)	1.2

Parameters are taken from Eppel et al. (1995) and references therein. Values given in brackets are used in SA2, and SM2, while the other values are applied in SA1, SM1 and in the snow-free areas of SA0 and SM0, respectively. Parameters denoted by * are calculated by the model.

3.7. Boundary conditions

The lower boundary condition of the snowpack is given by the ground-surface temperature, which is calculated by:

$$T_{ground} = T_{soil,1} - \frac{G_{ground}\Delta t}{\rho_s c_s \Delta z_{soil,1}}, \tag{25}$$

where $T_{soil,1}$ denotes to the soil temperature of the uppermost soil layer (see Fig. 2) and Δt is the time step. The heat diffusion equation is used to derive soil temperatures (see Claussen, 1988). Analogously, the snow-surface temperature, $T_{s,surf}$, is given by:

$$T_{s,surf} = T_1 - \frac{G_{snow}\Delta t}{\rho_1 c_i \Delta z_1}, \tag{26}$$

where T_1 stands for the snow temperature of the uppermost snow layer (see Fig. 2).

3.8. Water budget of the soil

If the snowpack drains water, this meltwater can be a source for soil moisture. Thus, the change in soil moisture reads (Fröhlich, 2001):

$$\frac{\partial f}{\partial t} = -\frac{E - P - M}{w_k \rho_w} + \frac{\alpha_c}{\rho_w}(1 - f), \tag{27}$$

where f is the soil wetness factor with $0 \le f \le 1$. The soil wetness factor equals the moisture content of the uppermost soil layer for which the moisture content has a diurnal cycle. It is the percentage of water that a sufficiently deep soil layer may take up before saturation occurs. The first term on the right-hand side represents the external forcing by evapotranspiration, E, meltwater outflow at the bottom of the snowpack, M ($= \mathrm{ul}_{z=0}$), and precipitation, P. Note that, in winter, vegetation rests for which transpiration is zero and

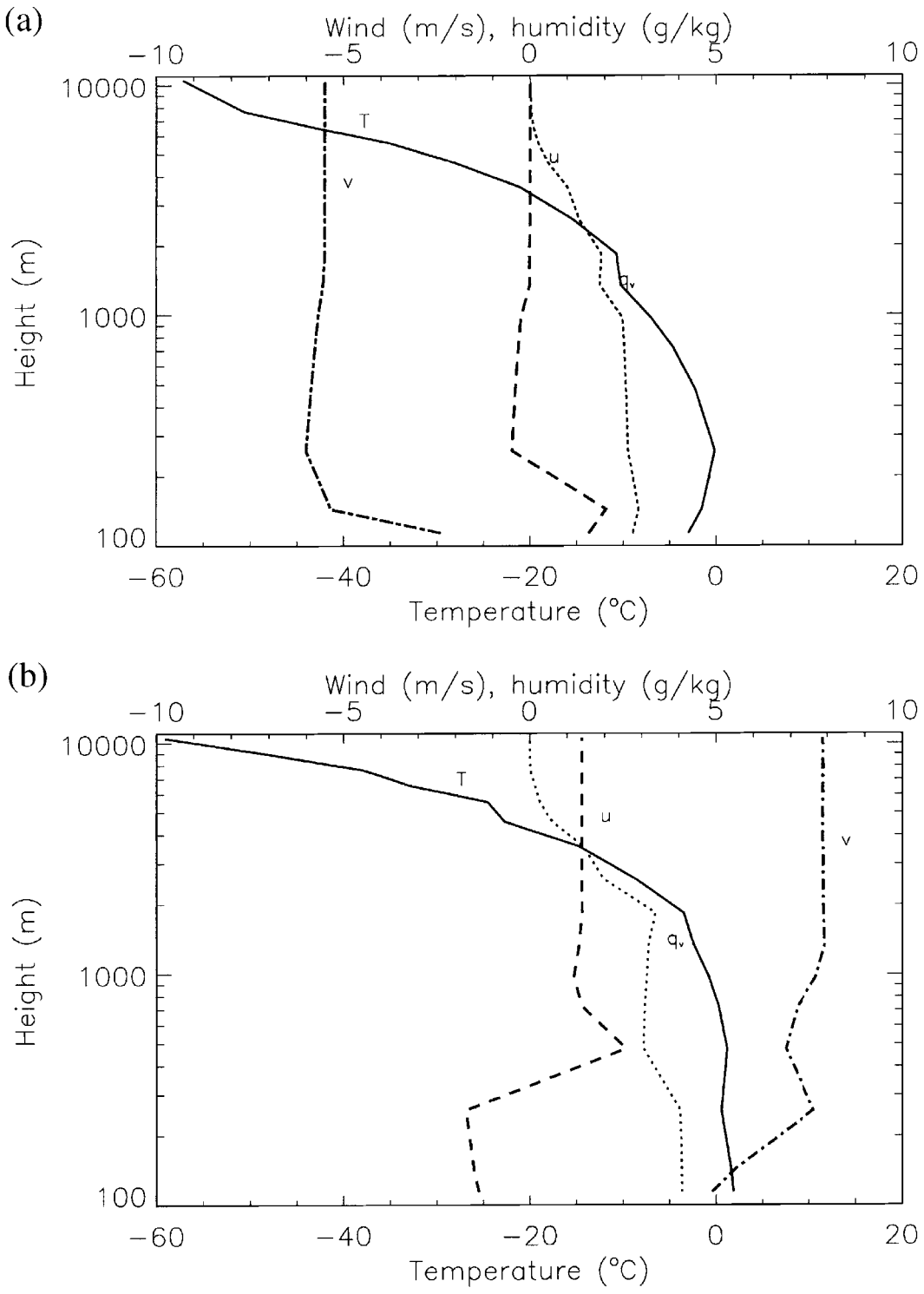

Fig. 3. Initial profiles of air temperature, humidity, *u*- and *v*-component of wind vector for the case study on (a) snow accumulation (SA*x*, $x = 0, 1, 2$), and (b) snowmelt (SM*x*, $x = 0, 1, 2$) as well as (c) initial distribution of snow depth for SM0. Note that initial snow depth is set equal to zero in SA0.

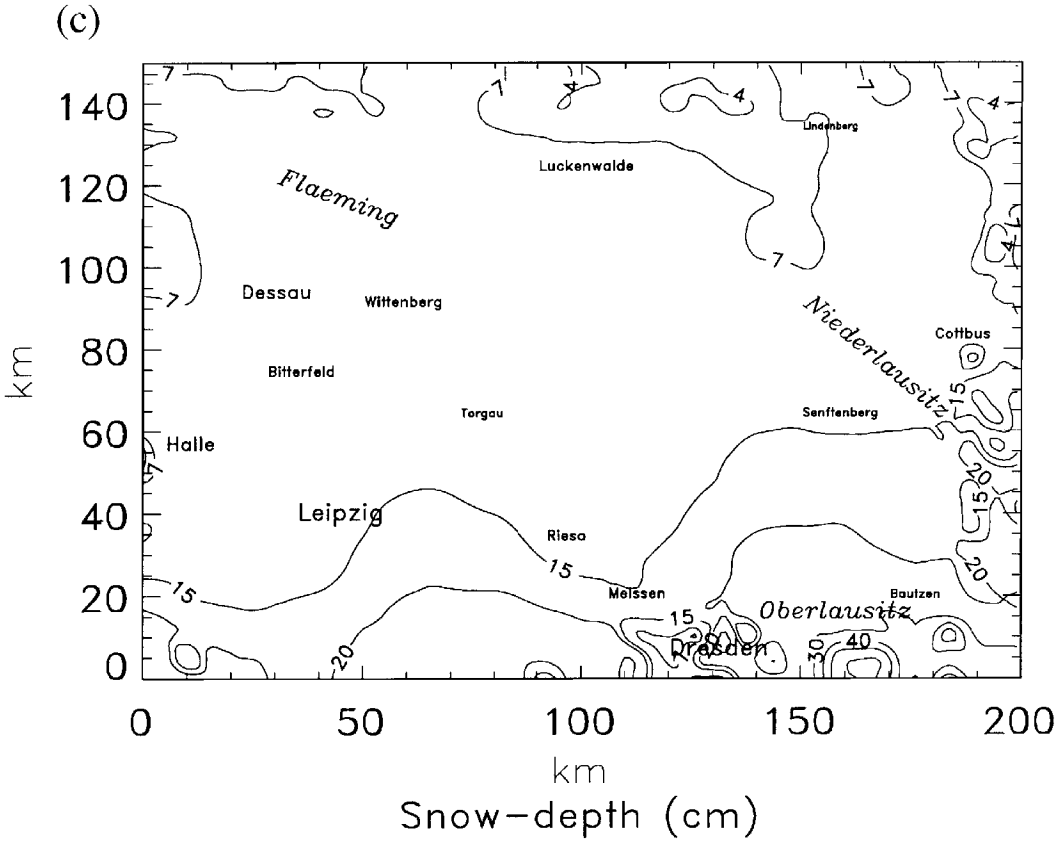

Fig. 3 (*continued*).

only evaporation of soil moisture exists. The last term of Eq. (27) stands for the restore of water from the ground-water layer into the upper soil layer. Field capacity weighted by the thickness of the uppermost diurnally active soil layer, w_k, and capillarity, α_c, are set equal to 1 m^3/m^3 and 1 kg/m^3 s in accord with Eppel et al. (1995).

4. Design of the study

4.1. Model domain and resolution

The model domain encompasses the troposphere over southern Brandenburg and northern Saxony (51°00N and 11°58E; 52°17N 11°53E; 51°N14°54; 52°17 14°49E; see Fig. 1). It extends 200 km in a east–west direction and 150 km in a south–north direction. The vertical resolution of the model varies from 20 m near the surface to 1 km at a height of 10 km above ground. Below and above a height of 2 km, there are eight levels. The horizontal grid spacing amounts to 5×5 km^2. The grid cells are assumed to be homogeneously covered by their individual vegetation over horizontally homogeneous soil types. According to the theory developed by Eagleson (1982) in which climate, soil and vegetation evolve synergetically, soil type is coupled to land-use type for purpose of simplicity (e.g., Eppel et al., 1995; Mölders, 1998, 1999a,b, 2000).

4.2. Initialization

The simulations start at each grid column with the same vertical profiles of wind, humidity, air and soil temperature (see Fig. 3). These profiles are attained by a dynamical initialization procedure wherein a 1D version of GESIMA adjusted the profiles to homogeneous terrain (in this case, agriculture, which has the largest fractional coverage within the model domain; cf. Fig. 1).

Simulations are carried out for a melting and an accumulation period. These simulations as well as their results are called SMx and SAx with $x = 0, 1, 2$. Here, 0 and 1 stand for the respective simulations with and without the snow model. The number 2 denotes to the sensitivity studies without snow model, wherein the values of albedo and emissivity are changed to those typical for snow (see Table 2). Note that representing snow by such a parameter modification means to take into account its radiative properties only. Other aspects like, for instance, the insulation or retarding of water input into the soils or rivers are neglected.

4.2.1. Case study on snowmelt

The impact of a melting snowpack is illustrated by simulating a typical snowmelt situation for mid-latitude flatlands. It was orientated at the one that occurred on 5 February 2001. At that time, the area of interest was snow covered. Warmer air masses were advected and led to snowmelt.

Since no data of the snow depth distribution are available in the resolution as required by GESIMA, the initial snow depth was arbitrarily assumed to be equal to 0.07 m over grass land, health and agriculturally used land, 0.15 m for all forest types, and 0.04 m for villages and cities at an elevation of 100 m above sea level (see Figs. 1, 3). Thus, the initial snow depth, $h_{\mathrm{s,initial}}$, of a grid cell is calculated from the snow depth prescribed at 100 m, $h_{\mathrm{s,vegtyp}}$, by the ratio of its elevation, z (in m), to the aforementioned 100 m:

$$h_{\mathrm{s,initial}} = h_{\mathrm{s,vegtyp}}\left(\frac{z}{100}\right), \tag{28}$$

to take into account that precipitation usually increases with elevation (e.g., Pleiss, 1977). Minimum and maximum initial snow depth amount to 0 above water and 0.60 m in forest in Oberlausitz, respectively (Fig. 3). For a distribution of terrain elevation, see Mölders (1999a).

Initial snow density is set equal to 100 kg m^{-3}, which is the value usually applied to calculate the water equivalent from the snow depth in hydrometeorological applications (e.g., Dingman, 1994). Furthermore, the snowpack is assumed to be isotherm at 273 K. Initial soil wetness factor, surface pressure, water-surface temperatures and soil temperatures, at 1 m depth, are set equal to 1, 1003 hPa, 277.2 K and 274.5 K, respectively. A geostrophic wind of 8.00 m/s from 260° represents the large-scale pressure gradient. The 24-h simulations start at 0000 UT.

The results of SM0, SM2 and SM1 are compared to each other. Special focus is on the differences that result from completely neglecting a snow cover and its effects at all (SM1) as commonly applied in models without snow model. In addition, we investigate how realistically the microclimate can be determined by a parameter change of albedo and

emissivity (SM2) as often applied in meso-β/γ-scale non-hydrostatic models (see, e.g., Eppel et al., 1995).

4.2.2. Case study on snow accumulation

To examine the impact of an accumulating snow coverage on local microclimate, 24-h simulations were performed starting at 21 February 1996 0600 UT with (SA0) and without the snow model (SA1, SA2). At that time, the synoptic situation was governed by a cyclone reaching from Mediterranean to Northeast Europe and an anticyclone located over North Atlantic. Over Mid-Europe, a low pressure system slowly moved southwards advecting arctic air masses. The pressure gradients led to snowfalls in the area of interest.

The water-surface temperatures and the soil temperature at 1 m depth were set equal to 277.2 and 274.5 K, respectively. An initial soil wetness factor of 1 and surface pressure of 1011.5 hPa were assumed. The large-scale pressure gradient is represented by a geostrophic wind of 5.50 m/s from 0°. The results of SA0, SA1 and SA2 are compared to each other as well as to routinely observed network data.

5. Results

5.1. Investigations on the performance in a stand-alone mode

5.1.1. Evaluation by means of analytical solutions

As aforementioned, the heat diffusion equation to determine snow temperatures is solved by an implicit Crank–Nicholson scheme in the standard version of the snow model (Fröhlich, 2001). To evaluate the prediction of snow temperatures, various simulations are carried out with the stand-alone version assuming different forcing of diurnal cycles of air temperatures and fixed ground temperatures (e.g., Fig. 4). In doing so, the temperatures are alternatively determined by the analytical solution, an explicit Richardson scheme and the implicit Crank–Nicholson scheme. Fig. 4 exemplary illustrates the results obtained by these three methods for the uppermost snow layer for an arbitrarily chosen forcing. Both numerical schemes require some time for spinup, but the implicit one reaches the analytical solution in half the time (about 16 h, on average) than required by the explicit one. Generally, the analytical and numerical solutions differ less than 0.2 K, with slightly lower differences (in the order of less than 0.01 K) for the implicit scheme than for the explicit one (e.g., Fig. 4). The phase of the diurnal cycle predicted by the implicit scheme agrees well with the analytical solution (e.g., Fig. 4). Furthermore, the implicit scheme is numerically more stable than the explicit one. For these two reasons, we chose the implicit scheme for the standard version of the snow model.

5.1.2. Evaluation of snow-depth prediction

To further examine the performance of the snow model, we use data from a routine network because there are no data of special field experiments that are continuously performed over several winters in flatland in mid-latitudes. Routine data, however, are of less accuracy compared to those gained in field campaigns. Moreover, some data that are required to feed the model are not recorded or are of imperfect quality. Therefore, an

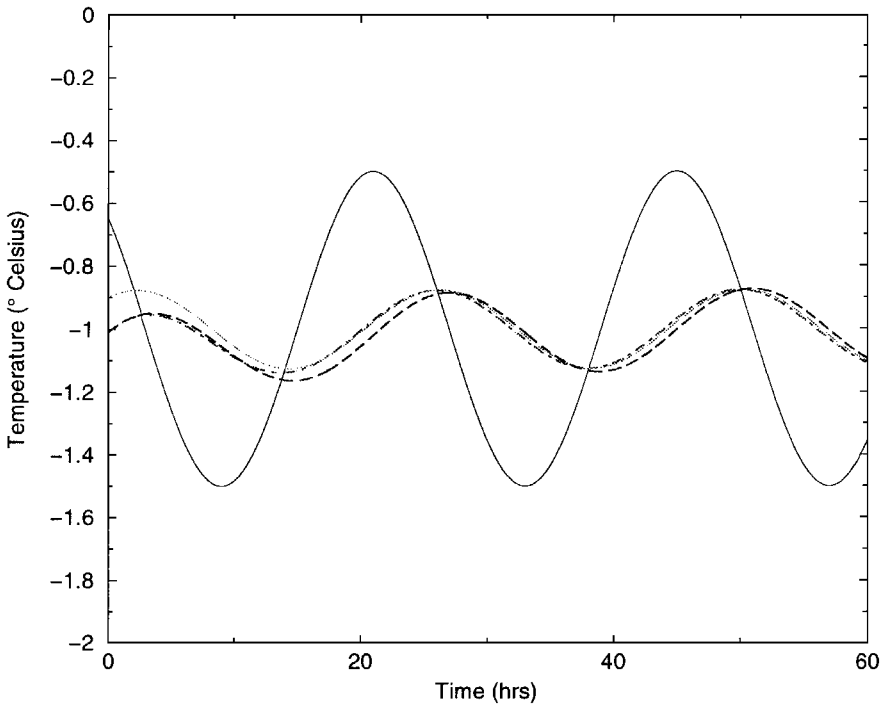

Fig. 4. Comparison of analytical and numerical solutions of the heat diffusion equation for a given external forcing (solid curve with large amplitude). The grey line, dash–dot line and dashed line stand for the analytical solution as well as for the solutions obtained by the implicit Crank–Nicholson scheme and the explicit Richardson scheme, respectively. Ground temperature was set equal to −5 °C.

evaluation by using routine data will never provide as good results as those that can be achieved when all needed data were measured under the special conditions of field campaigns (e.g., Spindler et al., 1996; Slater et al., 1998).

A stand-alone version of the snow model is driven by hourly data recorded at Brandis between 1993 and 1997. Air temperature and wind speed were logged at 2 and 10 m, respectively. Snow depth was measured once a day and snow-water equivalent was determined by melting of the snow fallen. The Brandis site is located in a rural environment where agriculture dominates. Since no data on soil-surface temperature are available, soil-surface temperature is assumed to be equal to air temperature.

The daily average of simulated snow depths are compared to the snow depth reported once a day. The snow model reproduces reasonably the temporal evolution of the snow depth; however, it slightly underestimates snow depth, on average (e.g., Fig. 5). Another important aspect of snow modeling is the timing of the end of a snowpack. In our analysis, we define the end of snowmelt as the first snow-free day predicted by the snow model after a snow episode. The times of the end of the snowpack agree well with the observations for short snow episodes with sometimes a retarding in the melting of about 1 or 2 days (see also Fig. 5). Note that the uncertainty of 1 day may be explained by the way of recording the data. If the snowpack is already melted at the time of observation, no snow is reported although there was snow on that day in the hours before recording. If for such a day the snow model still predicts snow and for the preceding day it predicts none, the snow model would be correct although the way of recording and averaging seemingly leads to the opposite result.

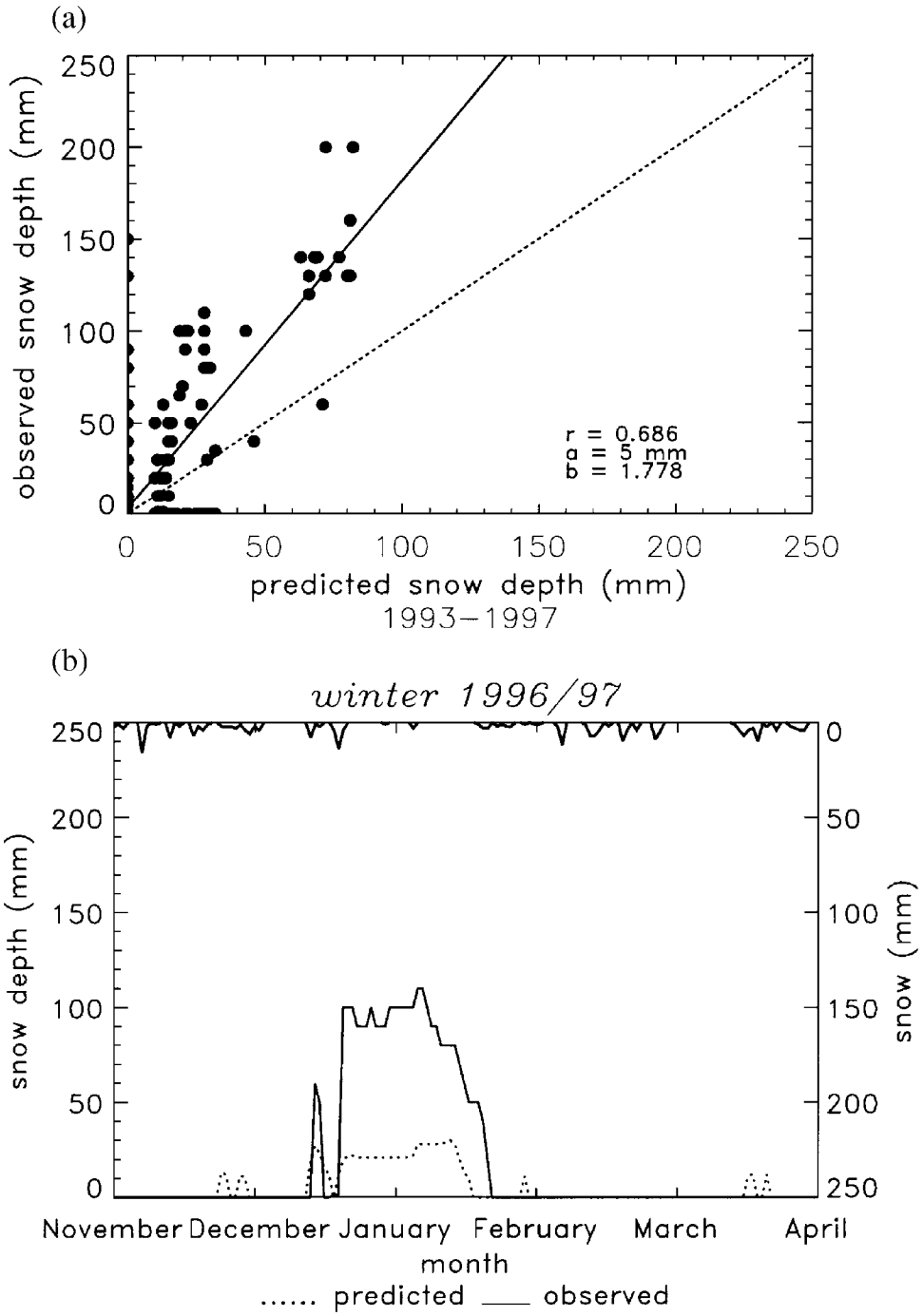

Fig. 5. Comparison of simulated and observed (a) daily snow depth for the snow events observed at Brandis during 1993 to 1997 and (b) a typical temporal course of snow depth during a cold season. Note that snow depths are shown for those days for which a snow event was reported, but data of snow depth were missing because it was unclear whether these data were just missing or whether no snowpack developed.

For long-lasting snow episodes, the snowpack melts too quickly (e.g., Fig. 5), which could be a hint that under such conditions the assumptions on soil-surface temperature become evident for the results. In nature, soil temperature decouples from air temperature during long snow episodes. As the atmosphere warms up, the soil-surface temperature will be still lower than air temperature. Setting soil-surface temperature lower than air temperature improves the timing of the disappearance of a snowpack after long-lasting snow periods.

Some discrepancies in snow depth may be explained by the errors in measured forcing data, the use of hourly meteorological and daily snow-depth routine data as well as by the lack of observations on other important quantities (e.g., soil-surface temperature, initial density of fallen snow flakes, soil albedo and emissivity, radiation, etc.) as well as by the abovementioned assumptions. The margin for error that typically arises in routinely measuring amounts to 0.2 K for air temperature and 0.5 m/s for wind (WMO, 1971). At air temperatures close to the freezing point, errors in air temperature may be decisive whether a snowpack melts or not. Errors in wind speed affect snow density and, hence, snow depth. Gage catch deficiencies nonlinearly increase with wind speed and may exceed 30% for a wind of 3 m/s (e.g., Dingman, 1994). Thus, the snow captured by the gage may differ from that actually fallen. Consequently, predicted snow depth may be underestimated because of too low input of snowfall when driving the snow model by the gage data. Sensitivity studies assuming a slightly increased snowfall manifest gage catch deficits as a possible source of the underestimation of snow depth by the snow model.

For some days, snowfall is reported, but snow depth is missing in the records (cf. Fig. 5). Since it is unclear whether there was snowfall, but no accumulation or whether the data are only missing, these days are included in Fig. 5 for completeness. On some days, appreciable snow depths were observed, but not simulated. Inspection of these days showed that snowfall was slight (about 1 mm/h) and long lasting at air temperatures around the freezing point. Thus, the accumulation did not exceed the critical value of 0.01 m in the snow model. The lack of recorded ground-surface temperature may also contribute to the fact that the snow model does not predict a snowpack under the aforementioned circumstances. Sensitivity studies, assuming colder-than-air temperature as ground-surface temperatures bring up snow depths for some of these days.

Discrepancies between simulated and observed snow depth may also result from the unknown density of the snow flakes. In the literature, values of snow flakes density range from 20 to 890 kg/m^3 (e.g., Fletcher, 1962; Zikumunda and Vali, 1972; Locatelli and Hobbs, 1974; Pruppacher and Klett, 1980). Sensitivity studies on the initial snow density demonstrated that the prediction of snow depth can be improved if initial snow density is chosen adequately, i.e., individually for each snowfall event.

As shown exemplary for the winter 1996/1997, observed snow depth can grow even without snowfall when deposited snow material is transported horizontally by the wind. Since the snow model does not consider this process, predicted and observed temporal evolution of snow depth differ under such circumstances (e.g., 26 December 1996 in Fig. 5).

5.2. Investigations on the performance of the snow model coupled to GESIMA

The data used in this comparison are point measurements from routine network usually taken over grass at station elevation. GESIMA, however, by design, predicts volume

averages of several square kilometers times the layer thickness in the case of air temperature and humidity (e.g., Kapitza and Eppel, 1992) as well as values representative for several square kilometers in the case of snow depth (Fröhlich, 2001). Measured near-surface meteorological quantities are not available at that scale. In reality, variations in the spatial features, such as topography, vegetation and soil type, exist, while in the model, a mean grid-cell elevation as well as a grid-cell representative soil and vegetation type are assumed. Therefore, any result that lies outside the range of error in the average, but falls within the observed scatter of measurement sites, should not necessarily be considered erroneous.

5.2.1. Case study on snowmelt

5.2.1.1. Snow depth, density and distribution. Snow density slightly grows by metamorphism. It varies between 84 kg/m^3 at the snow surface in areas of snowfall under calm wind to about 130 kg/m^3 close to the ground in areas of snowmelt. Snow depth decreases by the combined processes that make up snow metamorphism (e.g., Figs. 6, 7). Maximum decrease in snow depth amounts to 0.055 m for the 24 h of simulation (Fig. 6).

5.2.1.2. Snowmelt, soil moisture, snow and soil temperatures. In wide parts of the domain, the snowpack becomes nearly isotherm during the day with slightly higher (0.1–0.3 K) snow-temperature values in the lowest snow layer than in the uppermost one

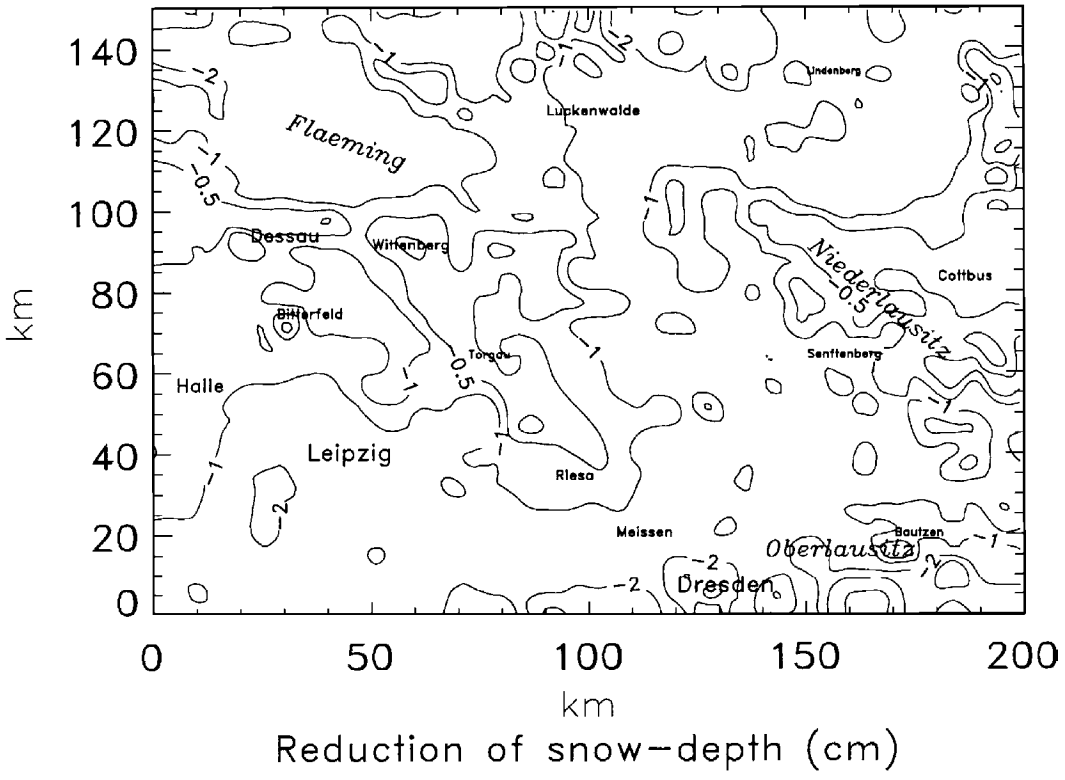

Fig. 6. Horizontal distribution of reduction in snow depth as obtained by SM0 for 0000 UT after 24 h of simulation.

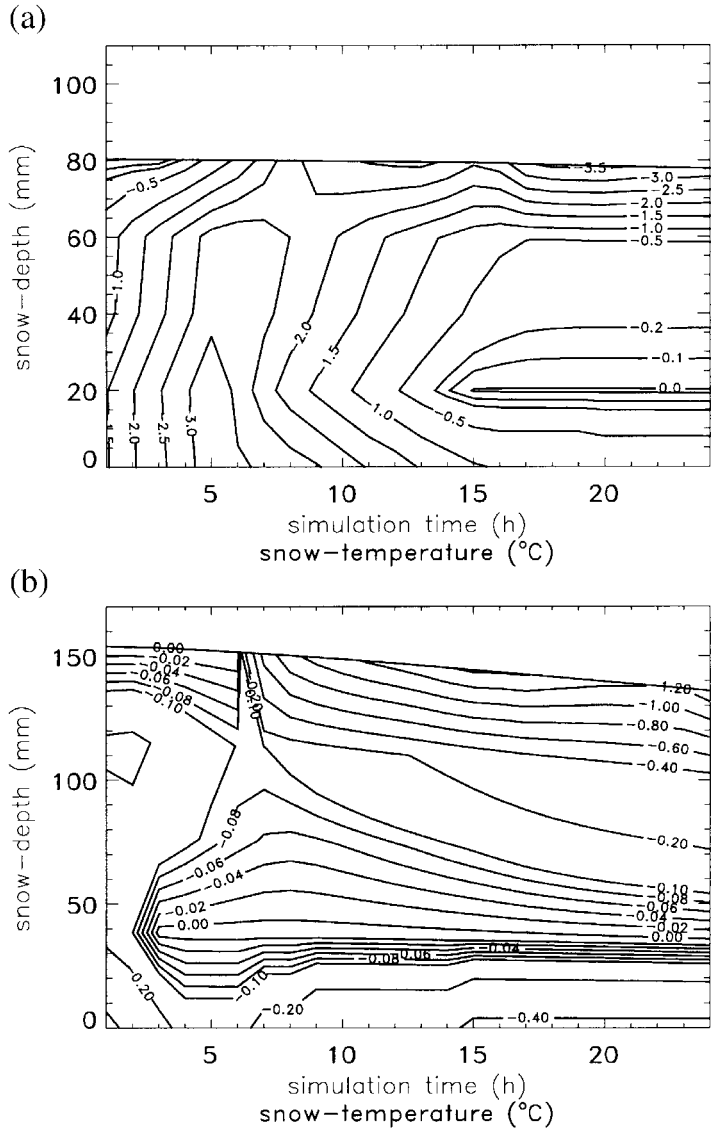

Fig. 7. Examples for the temporal evolution of snow temperature within the snowpack at: (a) 90 km in west–east and 70 km in south–north direction over grassland, and (b) 30 km in west–east and 30 km in south–north direction over Leipzig.

(e.g., Fig. 7). In the late afternoon, a noticeable temperature gradient establishes in the snowpack with warmer snow temperatures (around the freezing point) close to the ground. This gradient grows during night (e.g., Fig. 7).

In SM0, snowmelt starts after 2 h of simulation. Melting starts in the cities that are not of subgrid scale (e.g., Bitterfeld, Leipzig, Dresden; see also Figs. 7, 8). One hour later, retention capacity is exceeded and meltwater leaves the snowpack at some locations. At noon, meltwater leaves the snowpack in Fläming, over the open-pit mines south of Leipzig and in the western Niederlausitz, in the conurbation of Dresden as well as in most parts of southern Brandenburg (cf. Fig. 8). Since the soils are close to saturation, snowmelt hardly

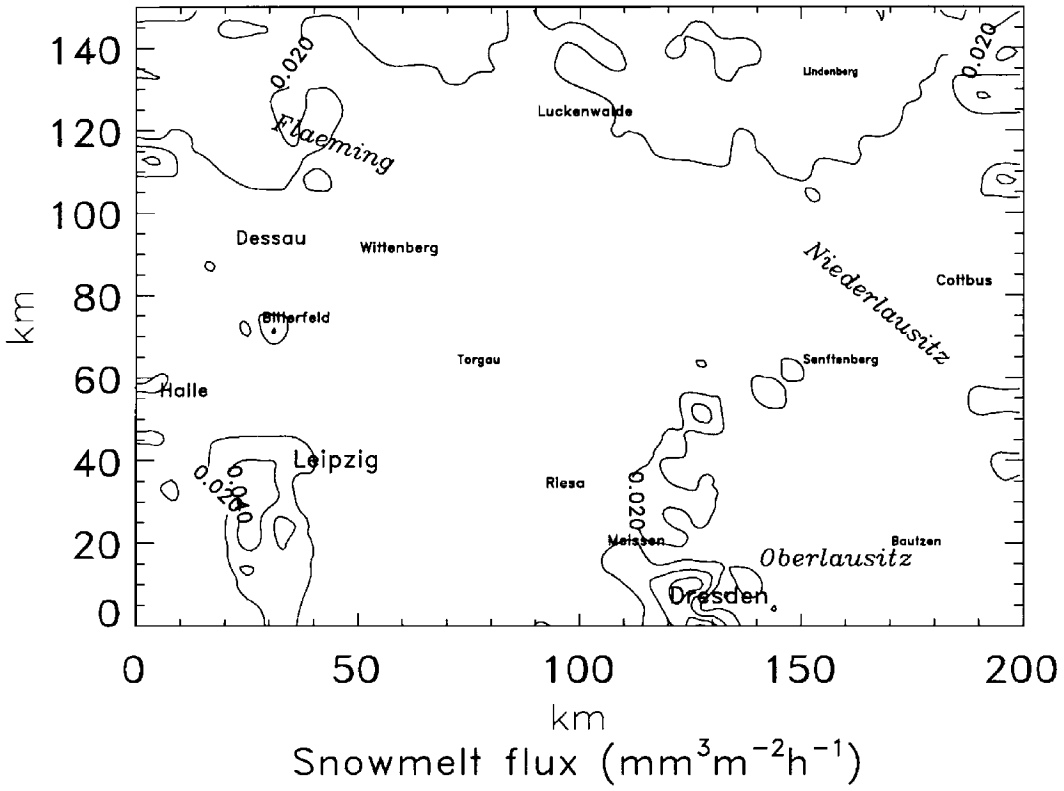

Fig. 8. Horizontal distribution of meltwater flux as predicted by SM0 at 1200 UT after 12 h of simulation.

affects soil wetness. In the evening, the snow temperatures decease (e.g., Fig. 7) for which melting is reduced or even stops in the rural sites.

Since the snowpack protects the soil from cooling, the soil-surface temperatures are appreciably higher in SM0 than in SM1 or SM2 (e.g., Fig. 9). At noon, for instance, minimum ground temperatures amount to -2.9, -6.4 and -7.4 °C for SM0, SM1, and SM2, respectively. The ground temperatures vary more strongly in SM1 and SM2 than in SM0, with the greatest variations occurring for SM1 (e.g., Fig. 9) because of its wider range of albedo and emissivity values (cf. Table 2). The differences in ground-surface temperatures between SM0 and SM1 or SM0 and SM2 increase as night progresses. On average, SM2 predicts the coldest soil surfaces (e.g., Fig. 9).

5.2.1.3. Air temperature and humidity. Differences between the air temperatures predicted by SM0 and SM1 (SM2) increase towards the surface. The temperature distribution of SM0 is more heterogeneous than that of SM1 or SM2 (e.g., Fig. 10). At noon, for instance, the near-surface layer is up to 4 K warmer in SM0 than SM1. Near-surface air temperatures range between -4.8 and 0.2 °C for SM0, -7.6 and -1.4 °C for SM1 as well as -8.3 and -2.3 °C for SM2, respectively. Just changing the surface albedo and emissivity (SM2) to typical values of snow leads to an about 2 K cooler near-surface atmosphere than SM1 at that time, i.e., 6 K colder than SM0 (e.g., Fig. 10). Since in the evening the atmosphere is only partly covered by very thin clouds, irradiance is great. As the ground surfaces are cooler in SM1 or SM2 than the snow surface in SM0 (e.g., Fig. 9),

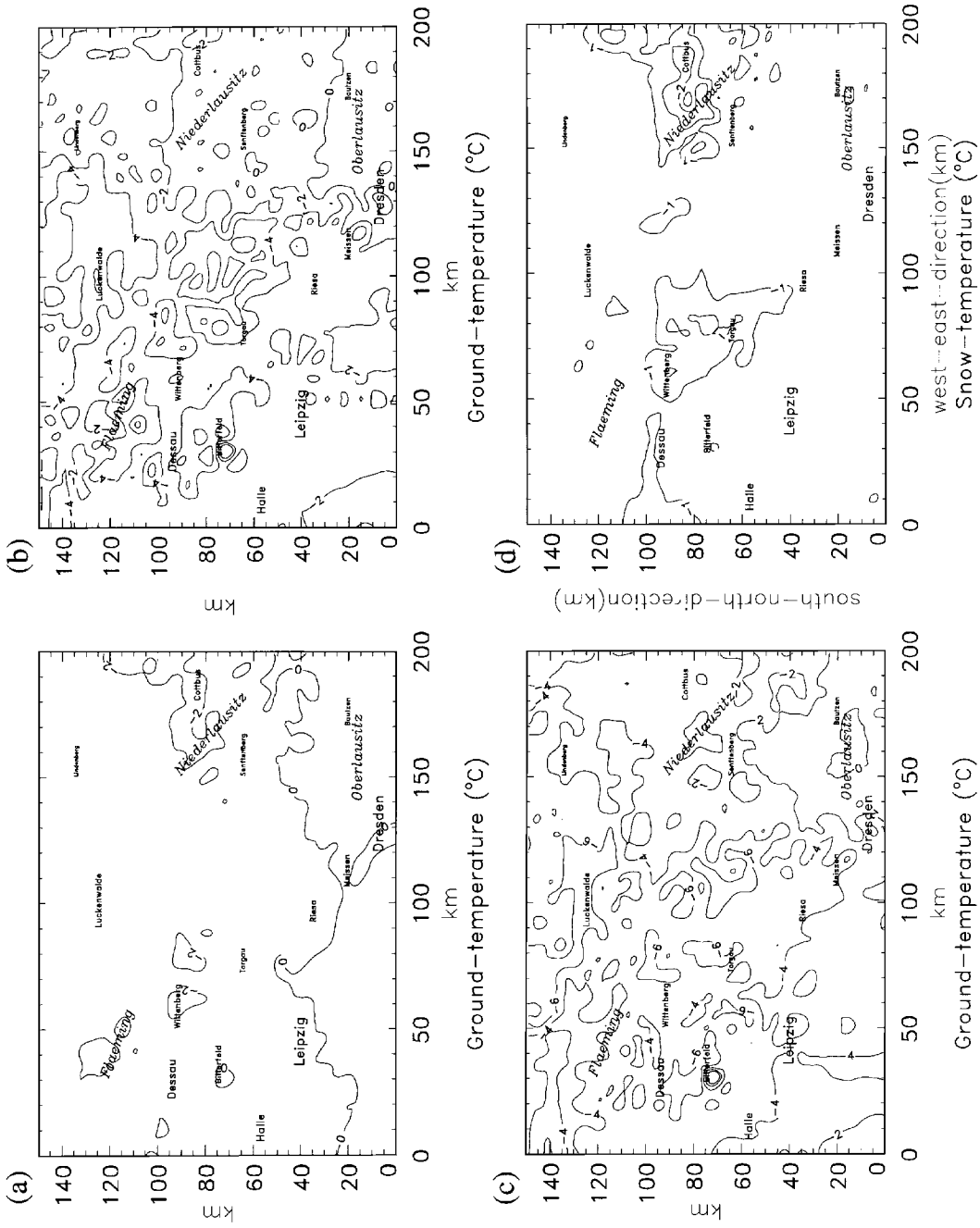
(a)
(b)
(c)
(d)
Ground−temperature (°C)
Ground−temperature (°C)
Ground−temperature (°C)
Snow−temperature (°C)
km
km
km
south−north−direction(km)
west−east−direction(km)
Flaeming
Niederlausitz
Oberlausitz
Dessau
Wittenberg
Luckenwalde
Leipzig
Halle
Riesa
Meissen
Dresden
Cottbus
Bautzen
Torgau
Bitterfeld
Lübben
Senftenberg

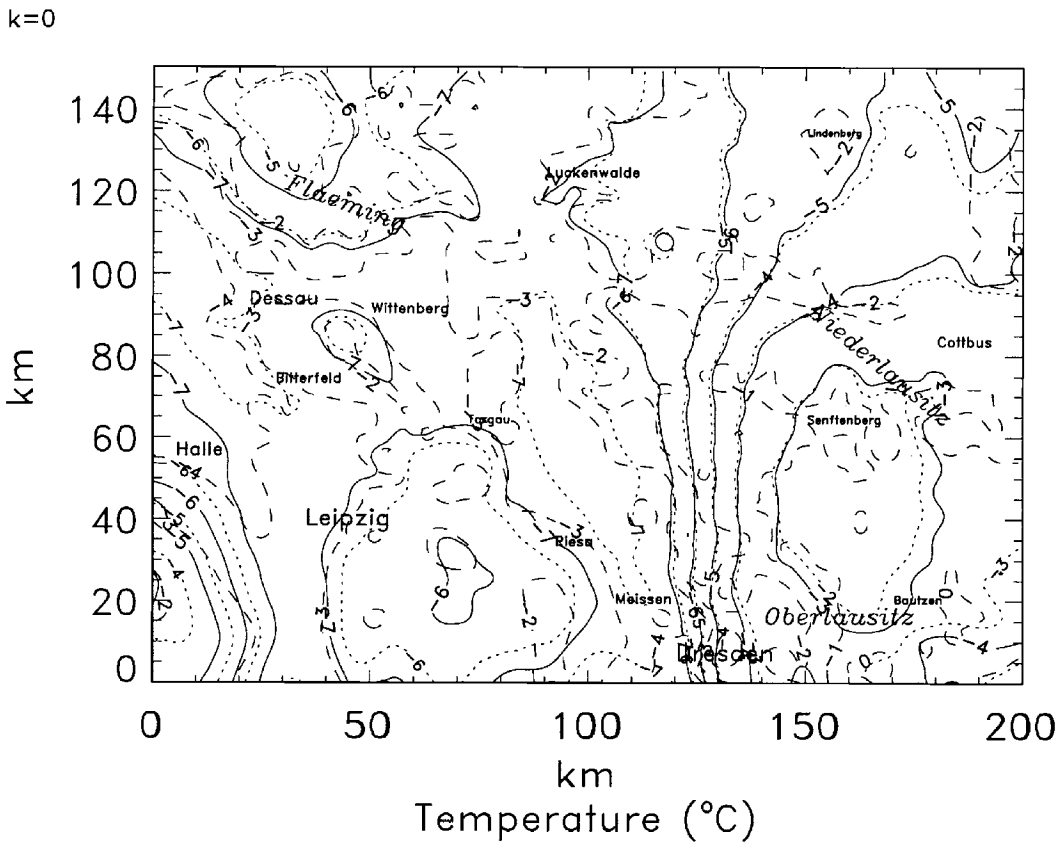

Fig. 10. Horizontal distribution of near-surface air temperatures as obtained with snow model (SM0, dashed lines), without snow model (SM1, dotted lines), and without snow model, but altered albedo and emissivity (SM2, solid lines) for 1200 UT after 12 h of simulation.

the near-surface atmosphere cools more in SM1 or SM2 and becomes more stable than in SM0.

In the surface layer, the specific humidity predicted by SM0 varies more strongly than that of SM1 (not shown). The difference in near-surface air temperatures contribute to those in humidity because a warmer atmosphere can hold more water than a colder one. Locally, specific humidity is more than 0.8g/kg higher in the surface layer of SM0 than SM1. Just changing the albedo and emissivity to typical values of snow (SM2) results in (e.g., 0.2 g/kg, on average, at noon) lower near-surface specific humidity than SM1, i.e., even lower than in SM0.

For both air temperature and specific humidity, the differences between SM1 and SM2 vanish in about 1 km above ground. Above the ABL, specific humidity and air temperatures predicted by SM1 (SM2) and SM0 slightly differ in cloudy regions due to difference in the consumption of heat or release of latent heat during phase transition processes.

Fig. 9. Horizontal distribution of ground surface temperatures as obtained: (a) with snow model (SM0); (b) without snow model (SM1) and (c) without snow model, but with altered albedo and emissivity (SM2) as well as (d) snow surface temperatures (SM0) for 1200 UT after 12 h of simulation. Note that close to Bitterfeld water is the dominant land-use type (cf. Fig. 1), which has a surface temperature of 4 °C.

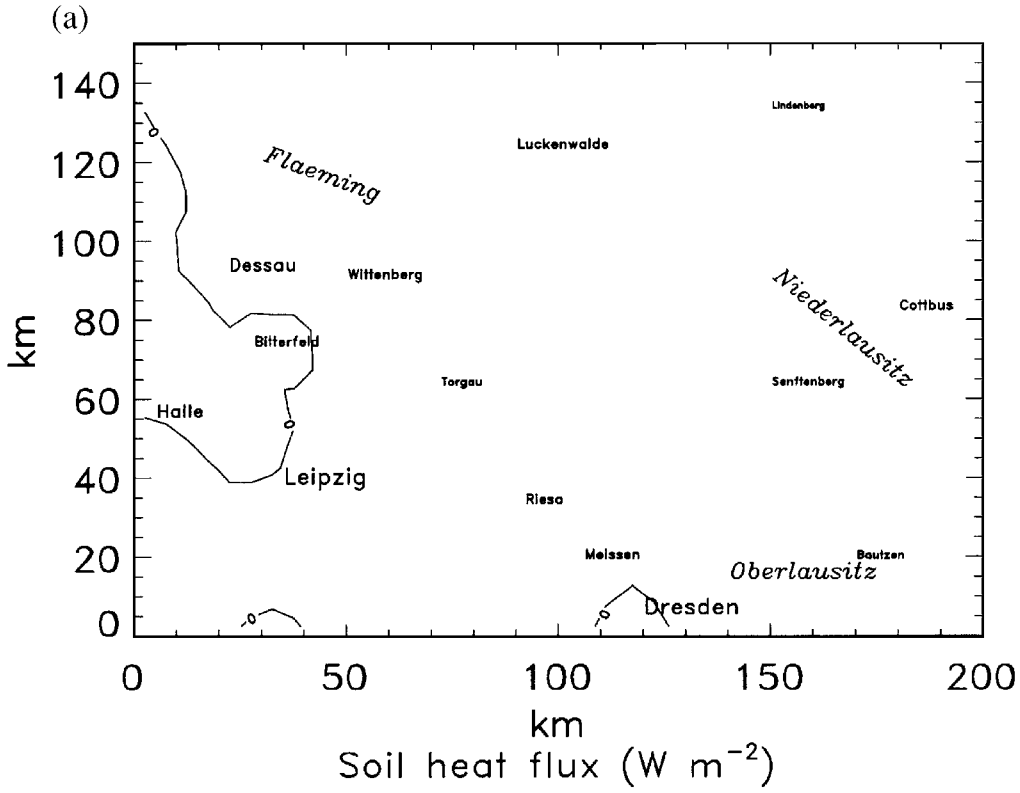
(a)
km
Soil heat flux (W m^{-2})
Flaeming
Luckenwalde
Lindenberg
Dessau
Wittenberg
Niederlausitz
Cottbus
Bitterfeld
Torgau
Senftenberg
Halle
Leipzig
Riesa
Meissen
Bautzen
Oberlausitz
Dresden

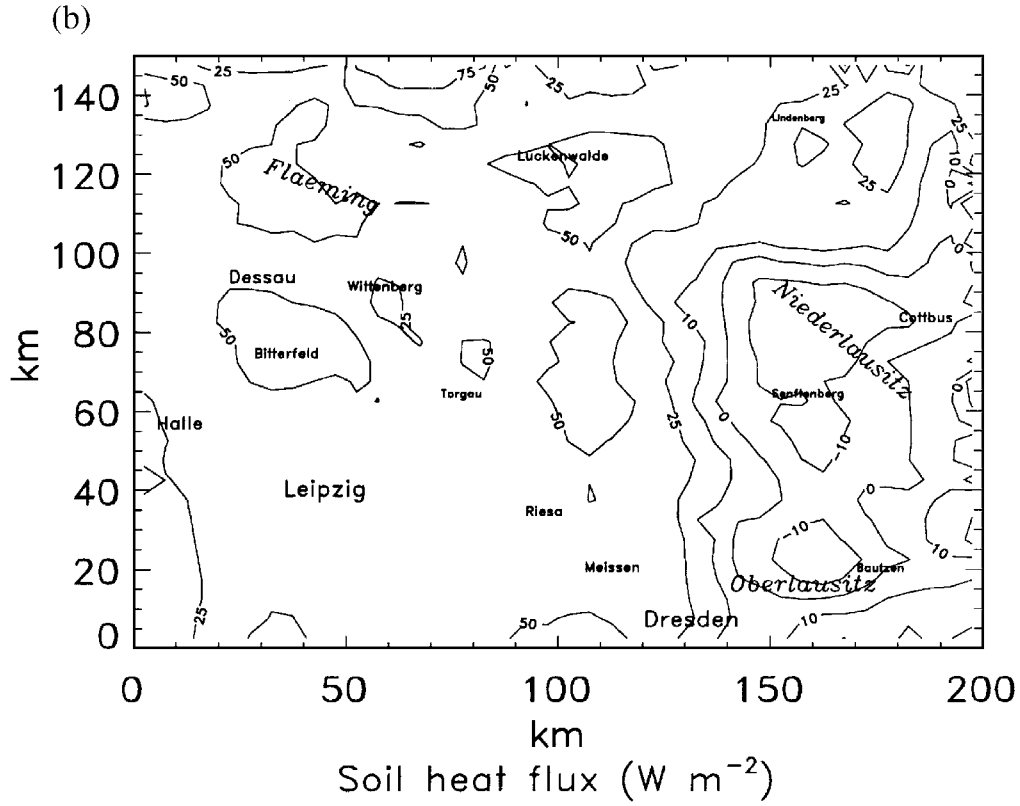
(b)
km
Soil heat flux (W m^{-2})
Flaeming
Luckenwalde
Lindenberg
Dessau
Wittenberg
Niederlausitz
Cottbus
Bitterfeld
Torgau
Senftenberg
Halle
Leipzig
Riesa
Meissen
Bautzen
Oberlausitz
Dresden

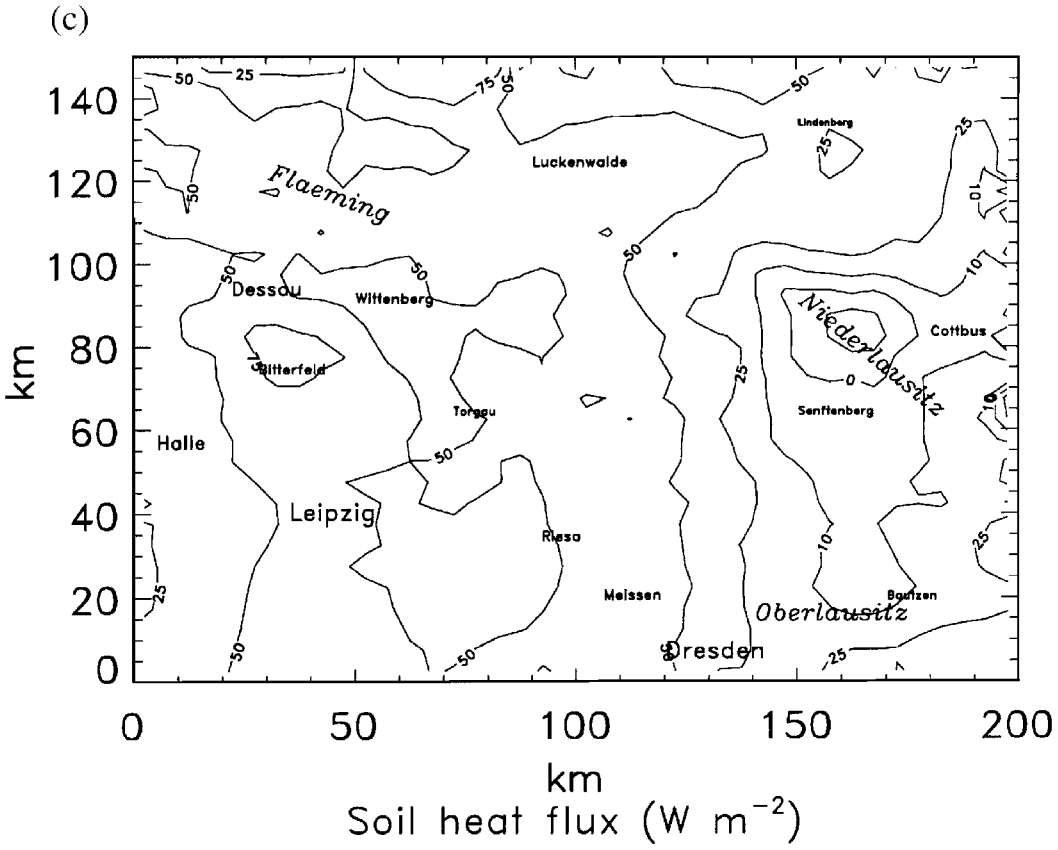

Fig. 11. Horizontal distribution of soil heat fluxes as obtained: (a) with snow model (SM0), (b) without snow model (SM1), and (c) without snow model, but altered albedo and emissivity (SM2) for 1200 UT after 12 h of simulation.

These findings mean that simulating snow effects by just changing the parameters of albedo and emissivity yields to the opposite effect than including both the physical processes and radiative properties of a snowpack. Thus, we may conclude that the insulating effect of snow has to be included in meso-β/γ-scale non-hydrostatic models to appropriately simulate the near-surface micrometeorological conditions (e.g., Figs. 9, 10).

5.2.1.4. Wind. In mid-latitudes in winter, the agriculturally used land and grassland have a low roughness length (Table 2). Therefore, in nature, snowfall does not modify roughness significantly except for very severe snow events. The high roughness of forests nearly keeps the same whether there is snow or not. For these reasons, snow does not alter roughness length in our study. Nevertheless, the inclusion of snow processes slightly affects the near-surface horizontal wind field (therefore, not shown). The different cooling of the atmospheric surface layer alters stratification and turbulent vertical mixing. Thus, the horizontal wind field changes in response to the altered vertical motions as required by continuity. In SM0, wind speed varies less than in SM1 or SM2, but it locally exceeds that of the other simulations by up to 1 m/s. Wind direction slightly changes as compared to SM1 or SM2.

(a)

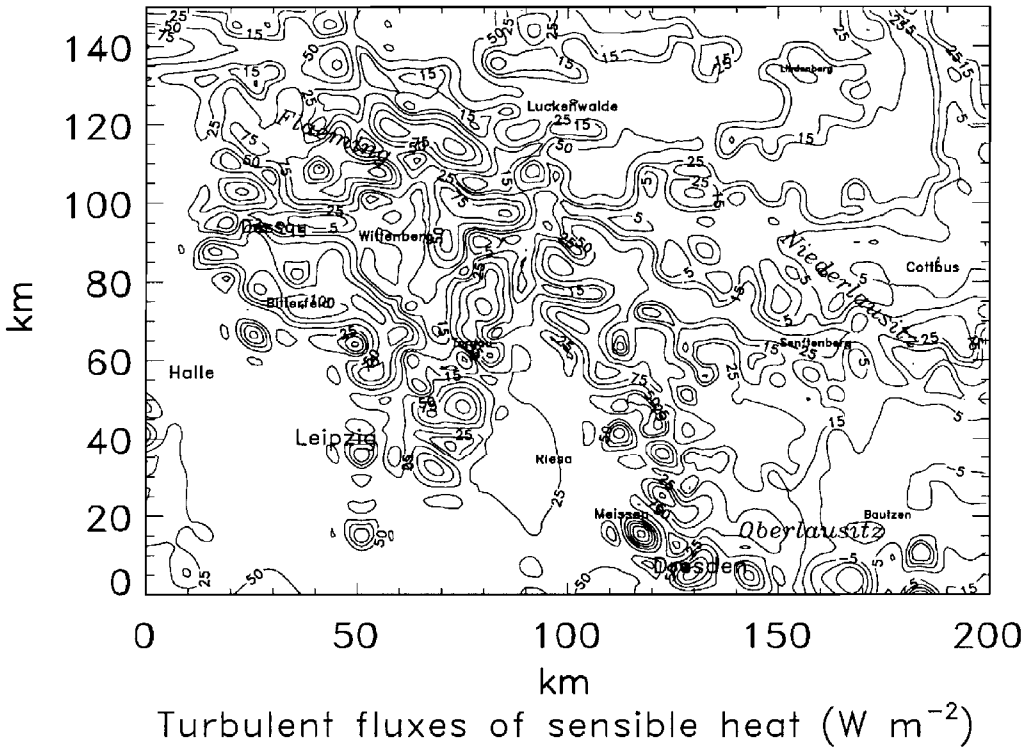
km
km
Turbulent fluxes of sensible heat (W m^{-2})
Halle
Leipzig
Dessau
Wittenberg
Bitterfeld
Luckenwalde
Fläming
Niederlausitz
Cottbus
Senftenberg
Riesa
Meissen
Bautzen
Oberlausitz
Dresden

(b)

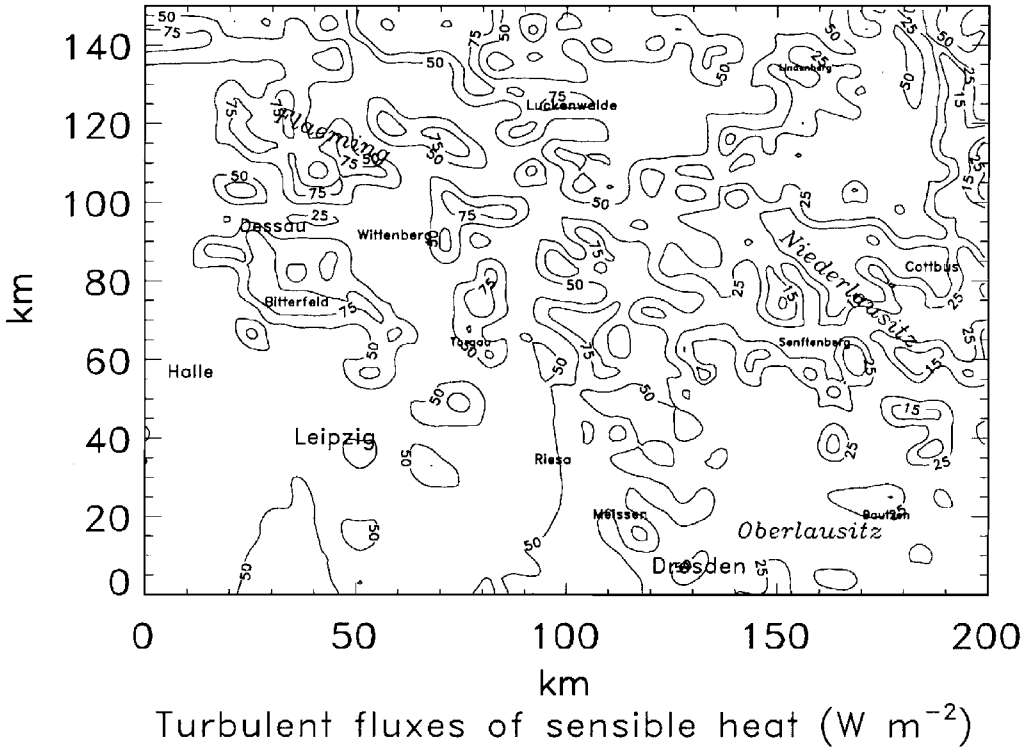
km
km
Turbulent fluxes of sensible heat (W m^{-2})
Halle
Leipzig
Dessau
Wittenberg
Bitterfeld
Luckenwalde
Fläming
Niederlausitz
Cottbus
Senftenberg
Riesa
Meissen
Bautzen
Oberlausitz
Dresden

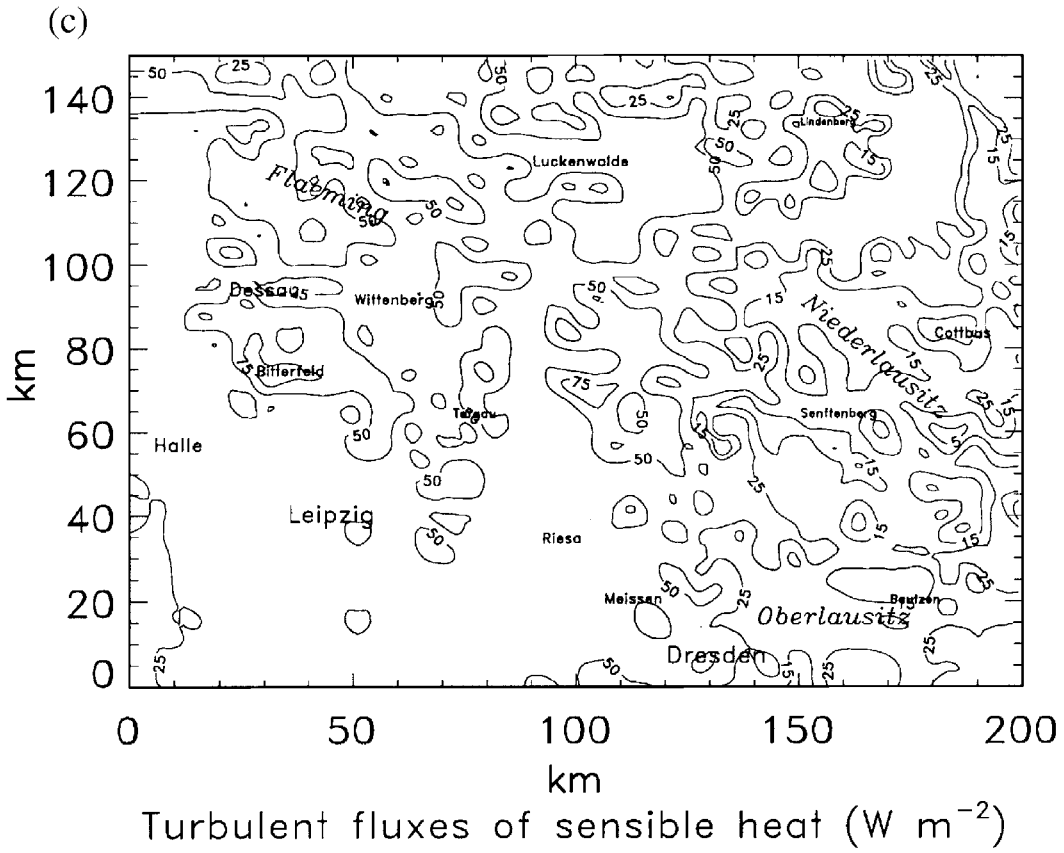

Fig. 12. Horizontal distribution of sensible heat fluxes as obtained (a) with snow model (SM0), (b) without snow model (SM1), and (c) without snow model, but altered albedo and emissivity (SM2) for 1200 UT after 12 h of simulation.

5.2.1.5. Fluxes. Due to the insulating effect of the snowpack (e.g., Fig. 9), soil heat fluxes slightly vary horizontally for SM0 (e.g., Fig. 11). On the contrary, there exists a strong horizontal variation of soil heat fluxes in SM1 or SM2. At noon, for instance, local maximum values amount to -10 and -70 Wm^{-2} in SM0, respectively, while predicted soil heat fluxes range between -32 and 120 Wm^{-2} for SM1 and between -24 and 131 Wm^{-2} for SM2. On average, SW2 delivers higher soil heat fluxes than SM1. The strength of predicted soil heat fluxes is closely related to soil type in SM1 and SM2 (e.g., Fig. 11), which should be the case in SM1 where snow is ignored at all. In reality, an important aspect of a snow cover is that soil heat fluxes are reduced. This effect is reproduced well by inclusion of the snow model (SM0), but it is not in the case when representing snow by emissivity and albedo values typical for snow (SM2).

At noon, the horizontal variability in sensible heat fluxes is the greater for SM0 (-39 to 183 Wm^{-2}) than for SM1 (7 to 84 Wm^{-2}) or SM2 (3 to 80 Wm^{-2}). The sensible heat fluxes are, on average, higher for SM1 than SM2 or SM0, with SM0 providing the lowest (e.g., Fig. 12). At noon, the latent heat fluxes predicted by SM0 exceed those of SM1 by up to 40 Wm^{-2} in the conurbation and in some areas of extended forest (e.g., Fig. 13). At

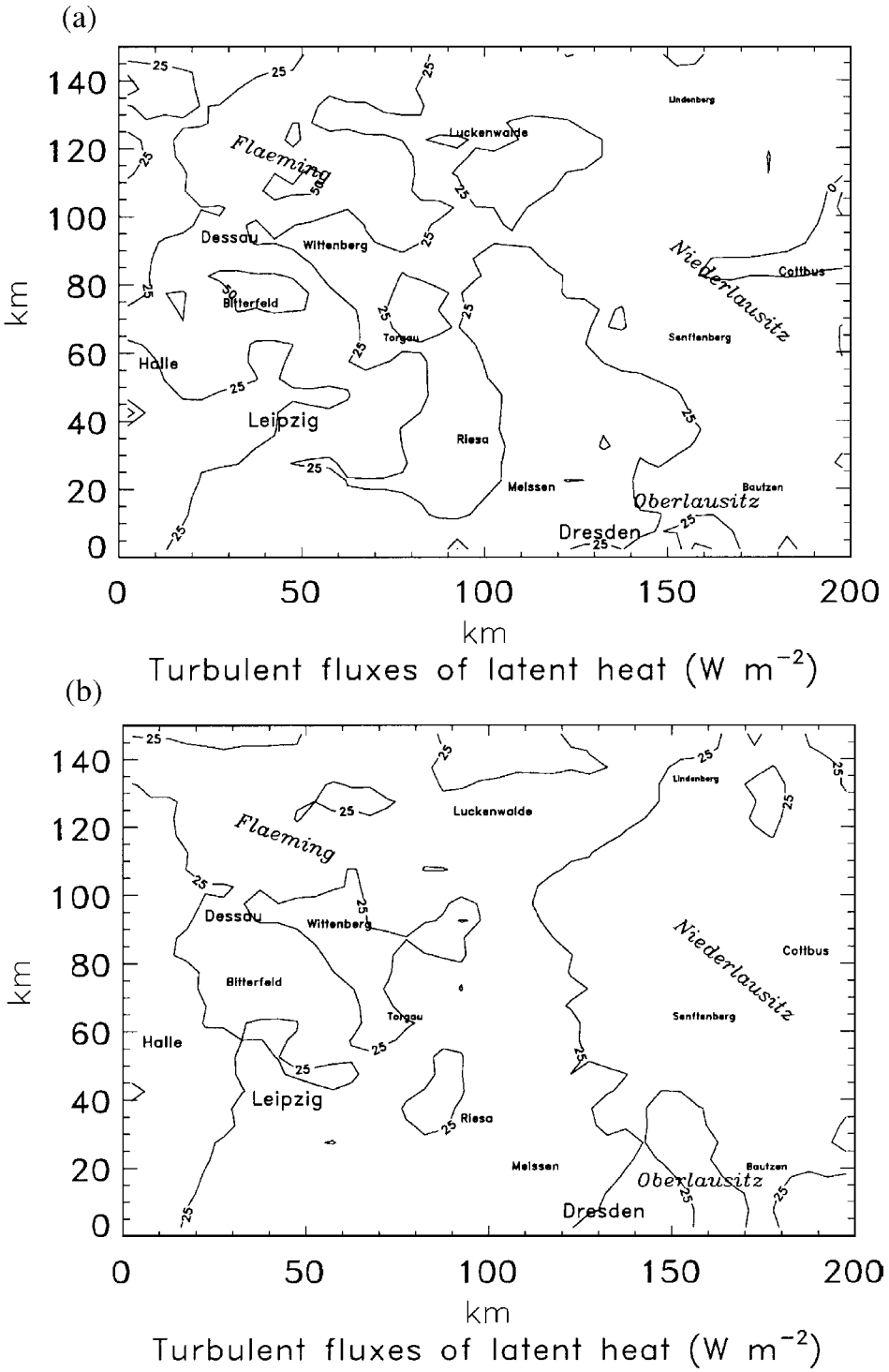

Fig. 13. Horizontal distribution of latent heat fluxes as obtained (a) with snow model (SM0), (b) without snow model (SM1), and (c) without snow model, but altered albedo and emissivity (SM2) for 1200 UT after 12 h of simulation.

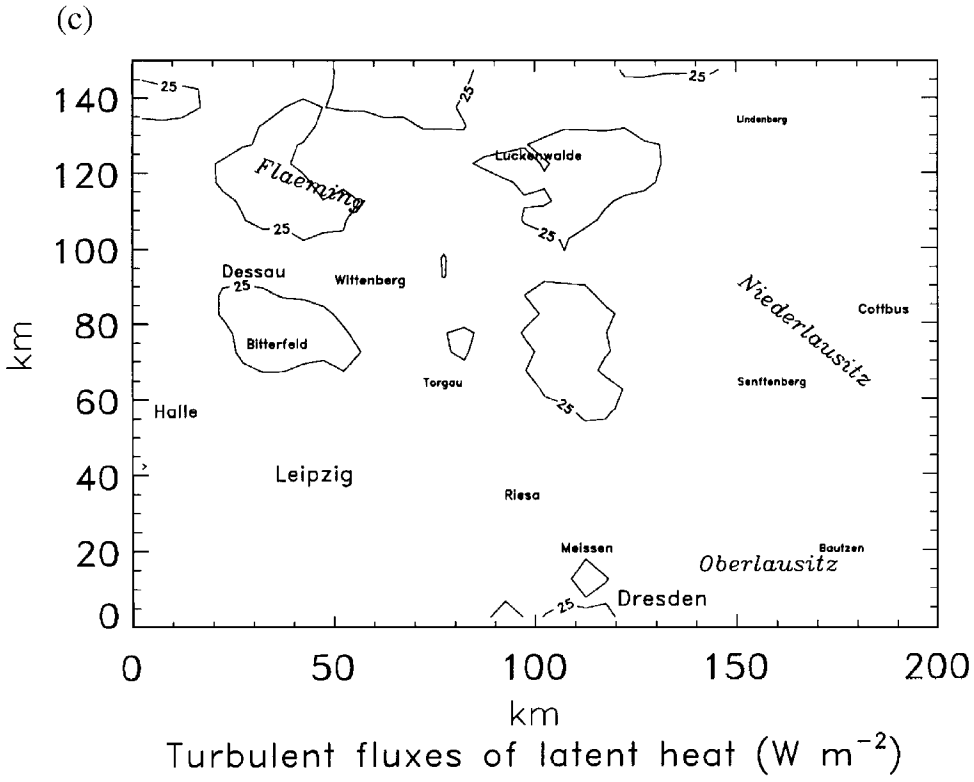

Fig. 13 (*continued*).

that time, the latent heat fluxes reach -7–127, 5–48 and 2–51 Wm^{-2} for SM0, SM1, and SM2, respectively. On average, SM0 predicts higher latent heat fluxes than SM1, followed by SM2. Like for the soil heat fluxes, the representation of snow just by altered albedo and emissivity leads to a change into the opposite direction than the inclusion of the explicitly modeled snow processes.

In summary, these findings indicate that the change in parameters alone is not sufficient to represent the soil heat fluxes and latent heat fluxes typically associated with snow conditions. Doing so even provides more unrealistic results than not considering snow at all.

5.2.2. Case study on snow accumulation

As indicated above, this case study examines the dramatic change in surface characteristic associated with the onset of a snow period and evaluates the model results by data from routine networks. SA0 and SA1 start with the same initial distributions of albedo and emissivity, while SA2 uses those typical for snow (Table 2). These initial values will be held constant over the entire simulation time in SA1 and SA2. In SA0, however, albedo and emissivity are calculated according to Eqs. (21) and (22) when snow depth exceeds 0.01 m, i.e., albedo and emissivity change in SA0 as compared to SA1. This critical depth is commonly assumed to be a threshold value at which low vegetation is totally covered by snow and at which snow metamorphism processes except melting become evident (e.g., Dingman, 1994).

5.2.2.1. Snow depth, density and distribution. It is obvious that mispredictions in simulated snowfall will lead to discrepancies in snow coverage and, consequently, snow depth (see also Foster et al., 1996; Raabe and Mölders, 1999). GESIMA predicts snowfall in the entire model domain in all three simulations. At 1300 UT, predicted snow depth reaches 0.01 m at some locations. At 2100 UT, it already exceeds 0.01 m in the area north of Dresden (between 80 and 150 km in west–east direction and 0 km and 50 km in south–north direction). At 0600 UT on 22 February 1996, Oberlausitz is covered by more than 0.01 m of snow (Fig. 14). At that time, maximum snow depth amounts to 0.22 m in Oberlausitz. The underestimation of snow extension with snow depths greater or equal to 0.01 m may be attributed to the fact that no cloud and precipitating particles are advected into the model domain. The latter means that clouds and precipitation need some time to be formed, onset of precipitation is retarded and less precipitation reaches the ground in the model as compared to nature.

Fig. 14 also illustrates the snow depth that would result by the assumption (e.g., Dingman, 1994):

$$h_s = \frac{\rho_w}{\rho_s} h_w = 10 h_w, \tag{29}$$

commonly applied in hydrometeorology. Here, h_w is the height of water equivalent of the accumulated snow and snow density is fixed to $\rho_s = 100$ km/m^3. This relationship provides unrealistically high snow depths in the areas of strong snowfall (cf. Fig. 14). In these areas, SA0 predicts snow depths of the same order of magnitude than observed (Fig. 14). The more realistic snow depths predicted by SA0 than SA1 (or SA2) can be explained by the fact that the wind strongly increases snow density from 84 kg/m^3 immediately after sedimentation to 424 kg/m^3 at maximum (cf. Fig. 15), while in determining snow depth according to Eq. (29), snow density keeps constantly at 100 kg/m^3. Note that the water equivalent of the predicted snowfall hardly differs between SA0 and SA1 or SA2 and, hence, negligibly contributes to the differences in snow depth. The three northernmost stations are located appreciably higher than the mean grid-cell height of the grid cells in which they are located. Since snow amount usually increases with elevation in the domain of interest, this discrepancy between the terrain height in the model and nature may also contribute to the misprediction of snow depth at these sites. In the conurbation of Leipzig, predicted snow depth is close to 0.01 m, but does not exceed this value. Here, the underestimation of snowfall leads to the misprediction of snow depth.

5.2.2.2. Soil moisture, snow and soil temperatures. The snow temperatures are nearly isotherm in the vertical with about -2 °C at maximum. In SA0, under the snowpack, ground-surface temperatures keep nearly constant with progressing time, i.e., the snowpack protects the soil from cooling. Here, the horizontal variation in ground-surface temperature mainly depends on (1) snow depth with stronger variations in areas of thin snowpacks, and (2) how long the snowpack already exists. Along the line of a snow depth of 0.01 m, huge horizontal gradients in surface temperatures exist. Soil moisture hardly changes in the snow-covered areas because no melting of snow and evaporation of soil moisture occur. In snow-free areas, the relative low evaporation negligibly alters soil moisture.

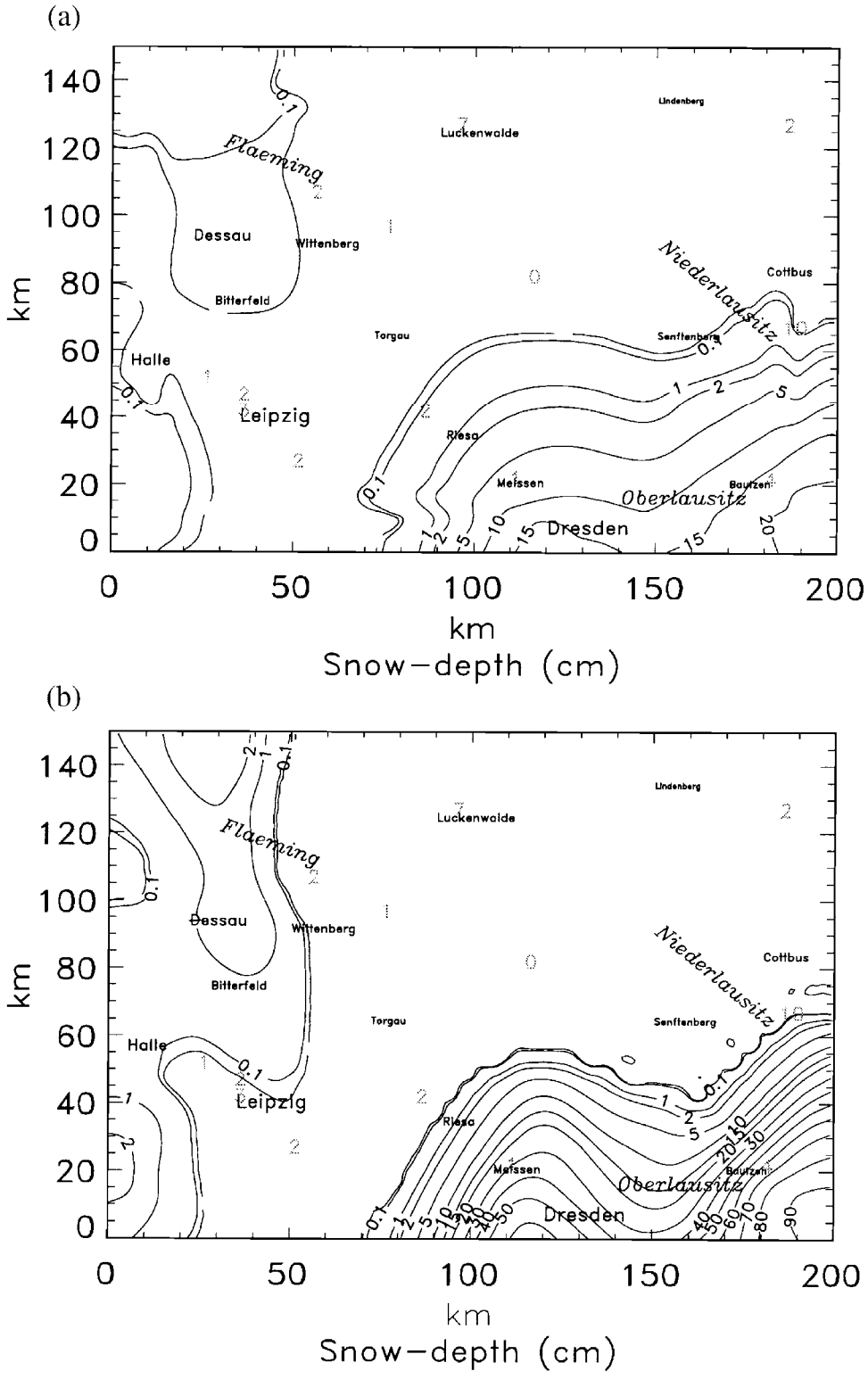

Fig. 14. Observed values are superimposed. Note that the snow distribution simulated by SA2 looks similar to that of SA1 (therefore, not shown).

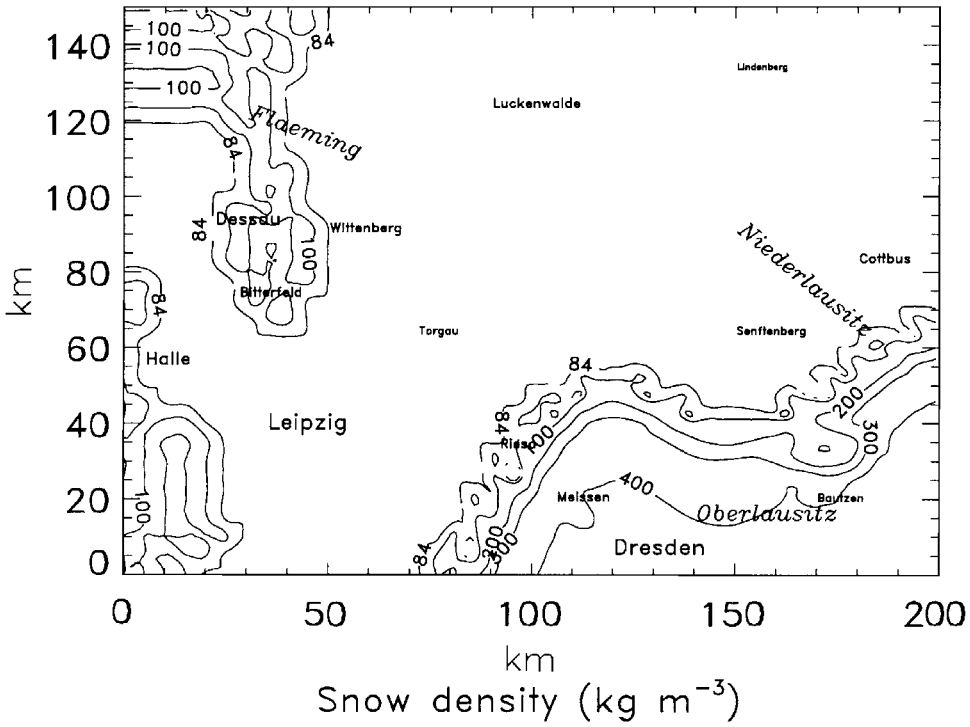

Fig. 15. Snow density in the uppermost snow layer as obtained by SA0 for 0600 UT after 24 h of simulation.

In the areas covered by more than 0.01 m of snow in SA0, appreciably lower soil-surface temperatures will be predicted if snow is only considered by a change in albedo and emissivity (SA2) or not at all (SA1). Consequently, in the area of sufficient snow depth, ground temperature varies less in SA0 than in SA1 or SA2, while in snow-free areas, SA1 and SA0 have a similar pattern. Note that the variation in ground temperature is associated with the different soil physical parameters that become relevant everywhere in SA1 or SA2 and only in the snow-free areas of SA0. Again, the representation of snow by modified values of albedo and emissivity leads to even lower ground temperatures than without any consideration of snow effects.

5.2.2.3. Air temperature and humidity. In the surface-layer, air temperatures predicted by SA0 are, on average, 0.6 K higher than observed except in the conurbation of large cities (e.g., Leipzig, Dresden). Here, predicted and observed air temperature differ up to 4.1 K at 1300 UT (Fig. 16). The dormitory villages are often of subgrid scale with respect to the model resolution for which their heating effect does not become evident in the simulation. Furthermore, in winter, anthropogenic heating by fuel combustion increases near-surface air temperatures by several Kelvin (e.g., Oke, 1978; Raabe et al., 1984). Note that differences of the same order of magnitude were found between Leipzig and its suburbs

Fig. 16. Comparison of simulated and observed near-surface air temperature and relative humidity at 2 m as obtained (a) with snow model (SA0), (b) without snow model (SA1), and (c) without snow model, but altered albedo and emissivity (SA2). Note that lower and left axis are for air temperature, while upper and right axis for relative humidity.

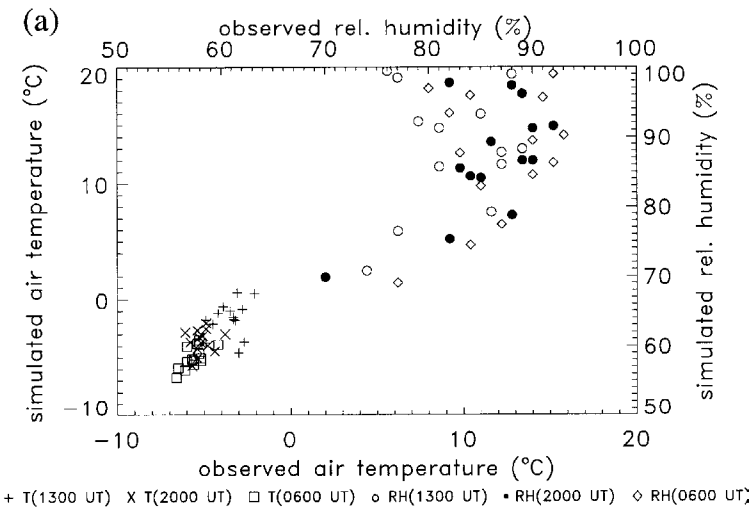
(a)
observed rel. humidity (%)
50 60 70 80 90 100
simulated air temperature (°C)
20 10 0 −10
simulated rel. humidity (%)
100 90 80 70 60 50
−10 0 10 20
observed air temperature (°C)
+ T(1300 UT) X T(2000 UT) □ T(0600 UT) ○ RH(1300 UT) • RH(2000 UT) ◇ RH(0600 UT)

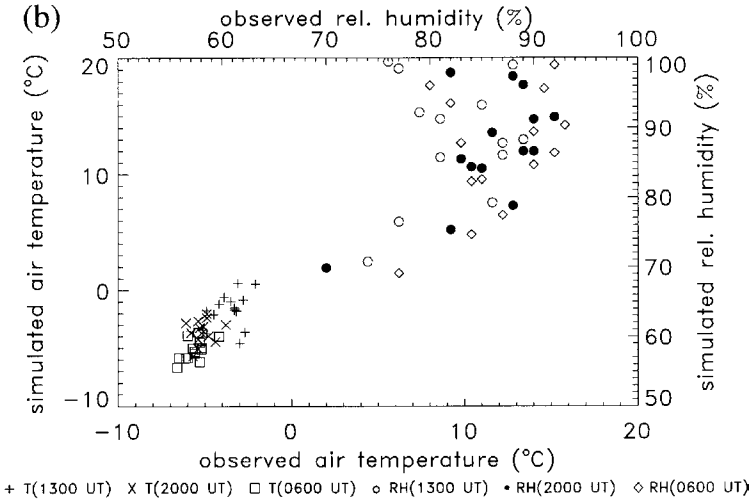
(b)
observed rel. humidity (%)
50 60 70 80 90 100
simulated air temperature (°C)
20 10 0 −10
simulated rel. humidity (%)
100 90 80 70 60 50
−10 0 10 20
observed air temperature (°C)
+ T(1300 UT) X T(2000 UT) □ T(0600 UT) ○ RH(1300 UT) • RH(2000 UT) ◇ RH(0600 UT)

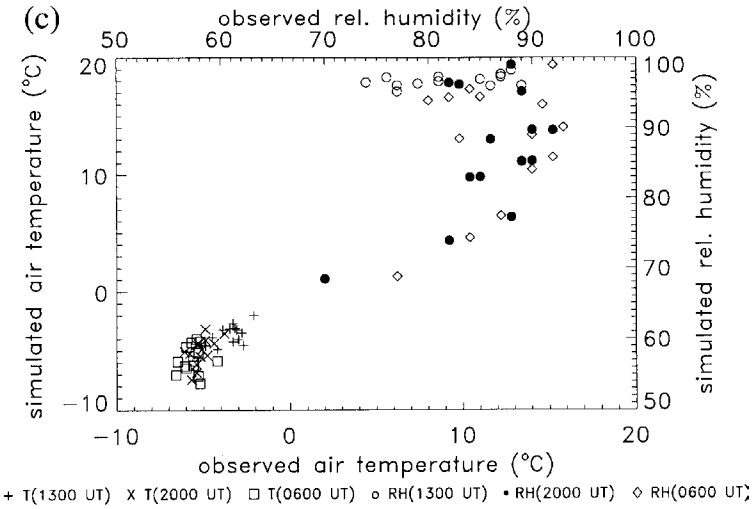
(c)
observed rel. humidity (%)
50 60 70 80 90 100
simulated air temperature (°C)
20 10 0 −10
simulated rel. humidity (%)
100 90 80 70 60 50
−10 0 10 20
observed air temperature (°C)
+ T(1300 UT) X T(2000 UT) □ T(0600 UT) ○ RH(1300 UT) • RH(2000 UT) ◇ RH(0600 UT)

under similar synoptic situations than those of our study (e.g., Raabe et al., 1984). It has to be expected that anthropogenic heating can be a sensitive quantity for initiation of snowmelt at near-surface air temperatures around freezing point. Errors in predicted cloud thickness and, hence, irradiation may be the reasons for the greater values of deviations. Air temperatures sink more strongly during night in the simulations without snow model than in that with snow model. SA1, on average, predicts 0.1 K higher air temperature than observed, while SA2 provides 1.5 K lower air temperatures than observed (e.g., Fig. 16). The correlation coefficients show that SA0 ($r = 0.730$) agrees slightly better with observation than SA1 ($r = 0.724$) or SA2 ($r = 0.694$). The mean rms error is 0.3 K for SA0 and SA1 and 0.2 K for SA2, respectively. Since typical values of rms errors of near-surface air temperatures in meso-α-scale models amount to 2.3 K after 24 h of simulation (Anthes et al., 1989), the prediction of near-surface air temperatures can be regarded as very good for all three simulations.

Relative humidity depends on air temperature. Thus, errors in that quantity propagate in the prediction of relative humidity for which the latter has greater prediction errors than air temperature, in general. All simulations overestimate the relative humidity in the near-surface layer (SA0 2%, SA1 3%, and SA2 5%, on average; e.g., Fig. 16). Here again, the great differences occur in the conurbation. In addition, great differences also exist when the model predicts snowfall at the time of observation, while in nature, the snowfall has stopped already. Thus, in the model, the environment becomes wetter than observed due to the sublimation from snowflakes during their settling. Above the snowpack, relative humidity is, on average, more than 2% higher in SA0 than in SA1. The overestimation of relative humidity by all three simulations can be partly explained by the assumption of a mass-weighted saturation mixing ratio. This assumption means that there can still be supersaturation with respect to ice when the temperatures are below freezing and both ice and super-cooled liquid water exist. In the case of a saturation mixing ratio with respect to ice, more moisture would be removed from the atmosphere and relative humidity (with respect to water) would be lower at air temperatures below freezing than for the mass-weighted saturation mixing ratio used here (Mölders et al., 1997; Mölder, 1999b). Again, correlation between predicted and observed values is better for SA0 and SA1 than SA2. The mean rms errors amount to 1.3% for the former two and 1.7% for the latter one.

In summarizing, the inclusion of the processes of snow metamorphism slightly improves simulated air temperatures and relative humidity as compared to the predictions without snow model.

5.2.2.4. Wind. Again, the horizontal wind field predicted by the simulation with snow model is slightly modified in response to the altered vertical motions as compared to those without (not shown due to the negligible differences).

5.2.2.5. Fluxes. As pointed out above, in SA0 over the snowpack, the values of albedo and emissivity differ from those at the same place in SA1, while in the snow-free areas, they are the same. In SA1 and SA2, the emissivity and albedo differ everywhere except for water (Table 2). These differences lead to primary differences in net radiation. Consequently, the incoming energy is partitioned differently between surface soil heat flux as well as the fluxes of sensible and latent heat. While these fluxes appreciably differ between

SA2 and SA1, they differ more strongly between SA1 and SA0 in the snow-covered areas. In the case of SA2 and SA0, the differences are the greatest in the snow-free areas of SA0. Since the insolation is already low in the evening when the snowpack gets an appreciable horizontal extension, the absolute discrepancies remain small (and smaller than those shown in Figs. 11–13). For soil heat fluxes, the greatest differences occur with more vigorous soil heat fluxes in SA1 (SA2) than in SA0 in those areas which are snow covered in the latter. These results again manifest that explicitly simulating snow processes is an urgent need also in meso-β/γ-scale modeling to adequately predict the surface fluxes and, consequently, soil surface and air temperatures. Neglecting of the insulating effect can lead to an unrealistically strong cooling of the soil even in short time.

6. Conclusions

A multiple-layer snow model to describe snow metamorphism is developed and coupled to the LSM of the meso-β/γ-scale non-hydrostatic model GESIMA to examine the impact of explicitly modeled snow processes on predicted local microclimate. An evaluation of the snow model is performed both in a stand-alone mode and within GESIMA. We evaluate the stand-alone version at the local scale by using data observed routinely at Brandis (51.32°N, 12.62°E, 133 m NN, Saxony) from 1993 to 1997. Although, on average, the snow model slightly underestimates snow depth, it reasonably predicts the temporal evolution of the snowpack depth. Discrepancies are due to errors in the meteorological forcing data, changes in snow depth by wind drift, gage catch deficits and the lack of other important quantities (e.g., soil-surface temperature, initial density of the snow flakes, albedo and emissivity of the soil, radiation, etc.). Predicted snow temperatures well agree to the analytical solution of the heat diffusion equation after some spinup.

In the coupled mode, simulations are exemplary performed with and without the snow model for a winter-storm snow event and a melting period in East Germany. The simulations without snow model are carried out alternatively with and without changing the values of albedo and emissivity to those typical for snow. Unfortunately, data for evaluation on the meso-β/γ-scale are scarce for snow as well as meteorological quantities. Thus, routinely measured data from networks are taken where available. These data of air temperatures and humidity provide evidence that the inclusion of the snow model improves the model performance as compared to the simulations without snow model. Accuracy of predicted snow depth, among other things, depends on the quality of the predicted distribution of snowfall, which is underestimated in our case study. Based on the few data available, however, we may conclude that the snow model predicts snow depth in the same order of magnitude as observed when predicted snow depth exceeds 0.01 m. The snow depths delivered by the snow model are more reliable than those calculated by relating snow depth to 10 times the height of the water equivalent to snow as often performed in hydrometeorology. The differences between simulated and observed snow coverage found for the coupled as well as for the uncoupled modes may be mainly addressed to the distribution of snowfall predicted by GESIMA.

Assuming values of albedo and emissivity typical for snow improves the prediction of the variables of state, water and energy fluxes as compared to simulations without such

changes. However, the evaluations evidence that some of the micrometeorological and microclimatological conditions, i.e., surface temperatures, near-surface air temperatures and humidity, latent heat fluxes, soil heat fluxes, etc., occurring in combination with a snowpack cannot be predicted adequately by just a change of albedo and emissivity. The explicit modeling of the insulating effect is essential for a realistic prediction of soil temperatures and surface fluxes. Based on our findings, we may conclude that snow models should be applied also in meso-β/γ-scale non-hydrostatic models as already done in climate modeling. It has to be expected that the discrepancies between the results from simulations with snow model and those representing snow by altered albedo and emissivity will be even greater in cold climate regions or under cooler synoptic situations than those investigated here.

A rigorous evaluation of the snow simulations within in coupled meso-β/γ-scale non-hydrostatic models requires datasets of snow cover extent, snow depth and snow water equivalent as well as meteorological quantities (variables of state, energy and water fluxes) in high quality and resolution for the entire model domain. Since such datasets are not yet available, a more detailed and overall evaluation has to be postponed to the future until such data are available.

Acknowledgements

We would like to express our thanks to K. Friedrich for digitizing the land-use data. We wish to thank DWD, U. Haferkorn, J. Döring, and U. Müller for access to the snow and meteorological data. We thank G. Kramm, and K.E. Erdmann as well as the anonymous reviewers for fruitful discussions and helpful comments. Thanks also to DFG and BMBF for financial support of this study under contracts Mo770/2-1 and 01LA9839/4, respectively.

References

Anderson, E.A., 1976. A point energy and mass balance model of snow cover. NOAA Technical Memorandum NWS Hydro-17. US Department of Commerce, Silver Springs, MD, p. 217.

Anthes, R.A., Kuo, Y.H., Hsie, E.-Y., Low-Nam, S., Bettge, T.W., 1989. Estimation of skill and uncertainty in regional numerical models. Q. J. R. Meteorol. Soc. 115, 768–806.

Baker, J.M., Davis, K.J., Liknes, G.C., 1999. Surface energy balance and boundary layer development during snowmelt. J. Geophys. Res. 104D, 19611–19621.

Blöschl, G., Kirnbauer, R., 1991. Point snowmelt models with different degrees of complexity—internal processes. J. Hydrol. 129, 127–147.

Cess, R.D., Poter, G.L., Zhang, M.-H., Blanchet, J.P., Chalita, S., Colman, R., Dezlich, D.A., del Genio, A., Dymikov, V., Galin, V., Jerret, D., Keup, E., Lacis, A.A., Le Treut, H., Liang, X.Z., Mahouf, J.H., McAvaney, B.J., Meleshko, V.P., Mitchell, J.F.B., Moncrette, J.J., Norris, P.M., Randall, D.A., Rikus, L., Roechner, E., Royer, J.F., Schlese, U., Sheinin, D.A., Slingo, J.M., Sokolov, A.P., Taylor, K.E., Washington, W.M., Wetherald, R.T., Yagai, I., 1991. Interpretation of snow-climate feedbacks as produced by 17 general circulation models. Science 253, 888–892.

Cherkauer, K.A., Lettenmaier, D.P., 1999. Hydrologic effects of frozen soils in the upper Mississippi river basis. J. Geophys. Res. 104D, 19611–19621.

Claussen, M., 1988. On the surface energy budget of coastal zones with tidal flats. Contrib. Atmos. Phys. 61, 39–49.

Colbeck, S.C., 1978. The physical aspects of water flow through snow. Adv. Hydrosci., 165–206.

Devantier, R., Raabe, A., 1996. Application of a quasispectral cloud parameterization scheme to a mesoscale snowfall event over the Baltic Sea. Contrib. Atmos. Phys. 69, 375–384.

Dickinson, R.E., Henderson-Sellers, A., Kennedy, P.J., 1993. Biosphere Atmosphere Transfer Scheme (BATS) version 1e as coupled to the NCAR Community Climate Model. NCAR Technical Note, NCAR/TN-378+STR.

Dingman, S.L., 1994. Physical Hydrology Macmillan, New York, 575 pp.

Douville, H., Royer, J.F., Mahouf, J.F., 1995. A new snow parameterization for the Meteo-France climate model: 1. Validation in stand-alone experiments. Clim. Dyn. 12, 21–35.

Dunne, T., Price, A.G., Colbeck, S.C., 1976. The generation of runoff from subarctic snowpacks. Water Resour. Res. 12, 677–685.

Eagleson, P.S., 1982. Ecological optimality in water-limited soil-vegetation systems: 1. Theory and hypothesis. Water Resour. Res. 18, 323–340.

Eppel, D.P., Kapitza, H., Claussen, M., Jacob, D., Koch, W., Levkov, L., Mengelkamp, H.-T., Werrmann, N., 1995. The non-hydrostatic mesoscale model GESIMA: Part II. Parameterizations and applications. Contrib. Atmos. Phys. 68, 15–41.

Essery, R., Martin, E., Douville, H., Fernández, A., Brun, E., 1999. A comparison of four snow-models using observations from an alpine site. Clim. Dyn. 15, 583–593.

Foster, J., Liston, G., Koster, R., Essery, R., Behr, H., Dümenil, L., Verseghy, D., Thompson, S., Pollard, D., Cohen, J., 1996. Snow cover and snow mass intercomparison of general circulation models and remotely sensed datasets. J. Clim. 9, 409–426.

Flerchinger, G.N., 1991. Sensitivity of soil freezing simulated by the SHAW model. Trans. ASAE 34, 2381–2389.

Fletcher, N.H., 1962. The Physics of Rain Clouds. Cambridge Univ. Press, London.

Fröhlich, K., 2001. Schneedeckenparametrisierung für ein mesoskaliges Modell. MSc thesis, Inst. Meteorol. Univ. Leipzig (in German; available from the author), p. 58.

Gao, X., Sorooshian, S., Gupta, H.V., 1996. Sensitivity analysis of the biosphere–atmosphere transfer scheme. J. Geophys. Res. 101D, 7279–7289.

Hermann, A., Kuhn, M., 1990. Schnee und Eis. In: Baumgartner, A., Liebscher, H.-J. (Eds.), Lehrbuch der Hydrologie, Band 1: Allgemeine Hydrologie - Quantitative Hydrologie. Gebrüder Bornträger, Berlin, Stuttgart, pp. 271–312.

Hinneburg, D., Tetzlaff, G., 1996. Calculated wind climatology of the South-Saxonian/North-Czech mountain topography including an improved resolution of mountains. Ann. Geophys. 14, 767–772.

Jin, J.M., Gao, X., Yang, Z.-L., Bales, R.C., Sorooshian, S., Dickinson, R.E., Sun, S.F., Wu, G.X., 1999. Comparative analyses of physically based snowmelt models for climate simulations. J. Clim. 12, 2643–2657.

Kapitza, H., Eppel, D.P., 1992. The non-hydrostatic mesoscale model GESIMA: Part I. Dynamical equations and tests. Contrib. Phys. Atmos. 65, 129–146.

Kongoli, C.E., Bland, W.L., 2000. Long-term snow-depth simulations using a modified atmosphere–land exchange model. Agric. For. Meteorol. 104, 273–287.

Kramm, G., Dlugi, R., Dollard, G.J., Foken, T., Mölders, N., Müller, H., Seiler, W., Sievering, H., 1995. On the dry deposition of ozone and reactive nitrogen compounds. Atmos. Environ. 29, 3209–3231.

Leavesley, G.H., 1989. Problems of snowmelt runoff modeling for a variety of physiographic and climatic conditions. Hydrol. Sci. J. 34, 617–634.

Levkov, L., Rockel, B., Kapitza, H., Raschke, E., 1992. 3D mesoscale numerical studies of cirrus and stratus clouds by their time and space evolution. Contrib. Atmos. Phys. 65, 35–58.

Locatelli, J.D., Hobbs, P., 1974. Fall speeds and masses of solid precipitation particles. J. Geophys. Res. 79, 2185–2197.

Loth, B., 1995. Die Schneedecke als Komponente des Klimasystems und ihre Modellierung. MPI f. Meteorol. Hamburg, No. 32. PhD thesis (in German; available from the author).

Loth, B., Graf, H.-F., Oberhuber, J.M., 1993. Snow cover model for global climate simulations. J. Geophys. Res. 98, 10451–10464.

Lynch-Stieglitz, M., 1994. The development and validation of a simple snow-model for the GISS GCM. J. Clim. 7, 1842–1855.

Marshall, S.J., Roads, O., Glatzmaier, G., 1994. Snow hydrology in a general circulation model. J. Clim. 7, 1251–1269.

Mellor, M., 1964. Properties of Snow. US Army Cold Regions Research and Engineering Laboratory Monogram III-AI, Hanover, NH, 105 pp.

Mölders, N., 1998. Landscape changes over a region in East Germany and their impact upon the processes of its atmospheric water-cycle. Meteorol. Atmos. Phys. 68, 79–98.

Mölders, N., 1999a. On the atmospheric response to urbanization and open-pit mining under various geostrophic wind conditions. Meteorol. Atmos. Phys. 71, 205–228.

Mölders, N., 1999b. On the effects of different flooding stages of the Odra and different land use types on the local distributions of evapotranspiration, cloudiness and rainfall in the Bradenburg–Polish border area. Contrib. Atmos. Phys. 72, 1–24.

Mölders, N., 2000. Application of the principle of superposition to detect nonlinearity in the short-term atmospheric response to concurrent land-use changes associated with future landscapes. Meteorol. Atmos. Phys. 72, 47–68.

Mölders, N., Laube, M., Kramm, G., 1995. On the parameterization of ice microphysics in a mesoscale α weather forecast model. Atmos. Res. 38, 207–235.

Mölders, N., Kramm, G., Laube, M., Raabe, A., 1997. On the influence of bulk-parameterization schemes of cloud microphysics on the predicted water-cycle relevant quantities—a case study. Meteorol. Z. 6, 21–32.

Mölders, N., Haferkorn, U., Döring, J., Kramm, G., 2001. Long-term numerical investigations on water budget quantities predicted by the hydro-thermodynamic soil vegetation scheme (HTSVS). In: Mölders, N. (Ed.), Untersuchungen zur regionalen Wasserverfügbarkeit unter veränderten Klimabedingungen. Report Mo770/2-1, pp. 267.

Oke, T.R., 1978. Boundary Layer Climates Routledge, London, 435 pp.

Orlanski, I., 1976. A simple boundary condition for unbounded hyperbolic flows. J. Comp. Physiol. 21, 251–269.

Pielke, R.A., 1984. Mesoscale Meteorological Modelling. Academic Press, London, p. 612.

Pleiss, H., 1977. Der Kreislauf des Wassers in der Natur VEB G. Fischer Verlag, Jena.

Pruppacher, H.R., Klett, J.D., 1980. Microphysics of Clouds and Precipitation Reidel, Dordrecht.

Raabe, A., Mölders, N., 1999. Evaluation of cloudiness and snowfall simulated by a semi-spectral and a bulk-parameterization scheme of cloud microphysics for the passage of a Baltic heat cyclone—first results. In: Raabe, A., Arnold, K., Heintzenberg, J. (Eds.), Meteorologische Arbeiten aus Leipzig (IV), Wiss. Mitt. Leipzig, vol. 12, pp. 59–70.

Raabe, A., von Hoyningen-Huene, W., Walter, A., 1984. Untersuchungen zum Wärmeinseleffekt einer Großstadt am Beispiel von Leipzig. In: Hänsel, C. (Ed.), Jahr. Allg. Umweltgeophys., 25–33 (in German; available from the authors).

Rodriguez, E., 1999. Surface modelling in HIRLAM, new scheme. Clim. Dyn. 9, 791–809.

Schlosser, C.A., Slater, A.G., Robock, A., Pitman, A.J., Vinnikov, K.Y., Henderson-Sellers, A., Speranskaya, N.A., Mitchell, K., PILPS2(D) contributors, 2000. Simulations of a boreal grass-land hydrology at Valdai, Russia: PILPS phase 2(d). Mon. Weather Rev. 128, 301–321.

Segal, M., Garratt, J.R., Pielke, R.A., Hildebrand, P., Rogers, F.A., Cramer, J., Schanot, A., 1991. On the impact of snow cover on daytime pollution dispersion. Atmos. Environ. 25B, 117–192.

Siemer, A.H., 1988. Ein eindimensionales Energie-Massenbilanzmodell einer Schneedecke unter Berücksichtigung der Flüssigwassertransmission, Berichte der Inst. f. Meteorol. u. Klimat. Der Univ. Hannover.

Slater, A.G., Pitman, A.J., Desborough, C.E., 1998. Simulation of freeze–thaw cycles in a general circulation model land surface scheme. J. Geophys. Res. 103D, 11303–11312.

Slater, A.G., Schlosser, C.A., Desborough, C.E., Pitman, A.J., Henderson-Sellers, A., Robock, A., Vinnikov, K.Y., Speranskaya, N.A., Michell, K., Boone, A., Braden, H., Chen, F., Cox, P., de Rosnay, P., Dickinson, R.E., Dai, Y.-J., Duan, Q., Entin, J., Etchevers, P., Gedney, N., Gusev, Y.M., Habbets, F., Kim, J., Koren, V., Kowalczyk, E., Nasonova, O., Noilhan, J., Schaake, J., Shmakin, A.B., Smironova, T., Verseghy, D., Weltzel, P., Xue, Y., Yang, Z.-L., 2000. The representation of snow in land-surface schemes: results from PILPS 2(d). J. Hydrometeorol., 1.

Spindler, G., Mölders, N., Hansz, J., Beier, N., Kramm, G., 1996. Determining the dry deposition of SO_2, O_3, NO, and NO_2 at the SANA core station Melpitz. Meteorol. Z. 5, 205–220.

U.S. Army Crops of Engineers, 1956. Snow hydrology. U.S. Department of Commerce Office of Technical Services PB 151660, Washington, DC.

Verseghy, D.L., 1991. CLASS—a Canadian land surface scheme for GCMs: I. Soil model. J. Clim. 11, 111–113.
Wanciewicz, A., 1978. A review of water movement in snow. Proc. on Modeling of Snow Cover Runoff. Proc. Banff Symp. US Army Cold Regions Research and Engineering Laboratory, Hanover, NH.
WMO, 1971. Guide to meteorological instrument and observation practice. WMO Rep. 8 TP3, 151 pp.
Yang, Z.-L., Dickinson, R.E., Robock, A., Vinnikov, K.Y., 1997. Validation of the snow submodel of the biosphere–atmosphere transfer scheme with Russian snow cover and meteorological observation data. J. Clim. 10, 353–373.
Yeh, T.-C., Wetherald, R.T., Manabe, S., 1983. A model study of the short-term climate and hydrologic effects of sudden snow-cover removal. Mon. Weather Rev. 111, 1013–1024.
Zhang, T., Stamnes, K., Browling, S.A., 2001. Impact of the atmospheric thickness on the atmospheric downwelling longwave radiation and snowmelt under clear-sky conditions in the Arctic and Subarctic. J. Clim. 14, 920–939.
Zikmunda, J., Vali, B., 1972. Fall patterns and fall velocities of rimed ice crystals. J. Atmos. Sci. 29, 1334–1347.